

# Coherent dynamics of flavor mode entangled neutrinos

---

Ashutosh Kumar Alok<sup>Ⓜ, a</sup> Massimo Blasone<sup>Ⓜ, b, c</sup> Trambak Jyoti Chall<sup>Ⓜ, a</sup>  
Neetu Raj Singh Chundawat<sup>Ⓜ, a, d</sup> Gaetano Lambiase<sup>Ⓜ, b, c</sup>

<sup>a</sup>*Indian Institute of Technology Jodhpur, Jodhpur 342037, India*

<sup>b</sup>*Dipartimento di Fisica, Università di Salerno, Via Giovanni Paolo II, 132 I-84084 Fisciano (SA), Italy*

<sup>c</sup>*INFN, Sezione di Napoli, Gruppo collegato di Salerno, Italy*

<sup>d</sup>*Institute of High Energy Physics, Chinese Academy of Sciences, Beijing 100049, China*

*E-mail:* [blasone@sa.infn.it](mailto:blasone@sa.infn.it), [chall.1@iitj.ac.in](mailto:chall.1@iitj.ac.in),  
[chundawat.1@iitj.ac.in](mailto:chundawat.1@iitj.ac.in), [lambiase@sa.infn.it](mailto:lambiase@sa.infn.it)

**ABSTRACT:** As the lynchpin of all quantum correlations, quantum coherence is fundamental for distinguishing quantum systems from classical ones and is essential for realizing quantum advantages in areas such as computation, communication, and metrology. In this study, we investigate the relationship between quantum coherence and neutrino oscillations by mapping the neutrino state as a multi-mode quantum system into qubit and qutrit frameworks. Our analysis extends beyond the commonly used  $l_1$ -norm and relative entropy of coherence to include all relevant measures of coherence such as robustness of coherence, coherence concurrence, trace-norm distance measure of coherence, coherence of formation, Schatten- $p$ -norm-based functionals, geometric coherence and logarithmic coherence rank, each offering unique insights into the quantum correlations in these systems. Notably, while the  $l_1$ -norm and relative entropy-based measures apply to general quantum states, the other measures are particularly relevant for entangled systems, highlighting the critical role of entanglement in neutrino oscillations. We present a detailed methodology for calculating coherence measures in both two-flavor and three-flavor mixing scenarios, contributing to a deeper understanding of how quantum coherence manifests and evolves in mode-entangled neutrino systems. Our findings emphasize the potential of these systems as robust candidates for quantum information tasks, facilitated by the weak interaction nature of neutrinos.

---

## Contents

<b>1</b>	<b>Introduction</b>	<b>1</b>
<b>2</b>	<b>Neutrinos as qubits and qutrit</b>	<b>4</b>
<b>3</b>	<b>Measures of quantum coherence</b>	<b>8</b>
3.1	$l_1$ -norm of coherence	9
3.2	Relative entropy of coherence	16
3.3	Schatten- $p$ -norm-based functionals	20
3.4	Geometric coherence as a fidelity-based measure	24
3.5	Logarithmic coherence rank	27
<b>4</b>	<b>Conclusions</b>	<b>29</b>
<b>5</b>	<b>Acknowledgements</b>	<b>32</b>
<b>A</b>	<b>Products of the coefficients <math>a_{\alpha\beta}(\theta_{ij}, L)</math></b>	<b>32</b>
A.1	Evaluation of $ a_{\alpha\beta}^*(\theta_{ij}, L) a_{\alpha\gamma}(\theta_{ij}, L) $ , $\beta \neq \gamma$	32
A.2	Evaluation of the probabilities $ a_{\alpha\beta}(\theta_{ij}, L) ^2$	34

---

## 1 Introduction

Neutrino oscillations are possible when two fundamental criteria are satisfied: first, the neutrino flavor state should be expressed as a linear combination of distinct mass eigenstates, and second, the temporal evolution of a flavor state must involve a coherent superposition of the time evolutions of the associated mass eigenstates. This coherent time evolution implies the presence of mode entanglement between the mass eigenstates constituting a flavor state [1, 2]. Thus, neutrino oscillations with three (or two) flavors can be studied by mapping the neutrino state as a three (or two)-mode system to a three (or two)-qubit system [3–8]. Another theoretically challenging scenario is when we map the neutrino states to more generic higher dimensional quantum systems like the three-level qutrit, in the case of three-flavor mixing [9, 10]. Consequently, neutrino oscillations are linked to the multi-mode entanglement of single-particle states, which can be described using flavor transition probabilities [4].

Over the past few decades, this concept of mode entanglement has been a focal point of intensive theoretical and experimental investigations, leading to a consensus that subspace entanglement is a fundamental feature of inter-particle interactions [11–29]. By providing various arguments, it was demonstrated in [11, 12] that the quantum state  $|\psi\rangle_{A,B} = |0\rangle_A \otimes |1\rangle_B + |1\rangle_A \otimes |0\rangle_B$ , where  $|0\rangle_A$  and  $|1\rangle_A$  (and similarly  $|0\rangle_B$  and  $|1\rangle_B$ )

represent states with zero and one particles in modes  $A$  and  $B$ , respectively is entangled and can display “single-particle nonlocality”. In refs. [13–20], it was proposed that this state can be used for applications such as teleportation, quantum cryptography, and testing Bell inequalities. Additionally, it is also possible to perform tomography on this state. In [20], it was demonstrated that teleportation using a single particle can be as reliable as using two particles, thereby dispelling doubts about the validity of single-photon entanglement as a resource in quantum information.

Numerous theoretical models and experimental realizations, particularly in atom-photon systems, have validated this concept, see for e.g., [16, 21–29]. The experimental realization of teleporting a one-particle entangled qubit was achieved in [21]. In this experiment, the qubit was represented by a mode of the electromagnetic field, where the orthogonal basis states  $|0\rangle$  and  $|1\rangle$  correspond to the vacuum state and the one-photon state, respectively. In Ref. [23], a single photon entangled with the vacuum was generated by directing a photon at a symmetric beam splitter. This entangled quantum state was then used to teleport single-mode quantum states of light utilizing the quantum scissors effect [30]. The experimental demonstration of single-photon nonlocality was carried out in [26] by utilizing a double homodyne measurement to assess correlations within the Fock space defined by zero and one-photon states. In [28], a coherent control scheme was presented to generate keV single-photon entanglement in nuclear forward scattering, where the spatial separation of the entangled field modes can be achieved using X-ray polarizers and piezoelectric fast steering mirrors.

In the context of neutrino oscillations, the principle of mode entanglement provides a framework for relating flavor oscillations to the bipartite or tripartite entanglement of single particle states. If such mode entanglement is demonstrated experimentally by spatially separating the modes [1], it could open new avenues for performing various quantum information tasks, thereby providing an alternative path to advancing quantum technologies. Neutrinos, interacting primarily through weak interactions, enable unique applications over vast distances and dense media due to negligible dissipation or scattering effects. For instance, it has been demonstrated that the teleportation fidelity of mode-entangled oscillating neutrino systems consistently exceeds the classical threshold, highlighting their potential for quantum teleportation [4]. Utilizing the weak interaction nature of neutrinos, such teleportation could be achieved across extensive barriers, such as mountains or even the entire Earth.

In this context, it is crucial to characterize neutrino flavor oscillations by examining various facets of quantum correlations in three (or two)-qubit as well as qutrit systems. Numerous studies have already examined quantum correlations in neutrino oscillations within the framework of two- and three-qubit along with qutrit systems, see for e.g., [1–10, 31–43]. These studies have investigated various aspects of quantum correlations, including non-locality quantified in terms of Bell, Mermin and Svetlichny inequalities along with the non-local advantage of quantum coherence [5, 7], entanglement quantified in terms of von Neumann and Shannon entropies and also nonlinear witness of genuine multipartite entanglement along with other measures such as concurrence, entanglement of formation and negativity [1, 4, 5], discord in terms of geometric discord [4], and dissension [5].

Quantum coherence is the defining feature that sets quantum states apart from classical states. It represents the core attribute of quantum mechanics, rooted in the universal principle of superposition, which is inherently nonclassical. In the fields of quantum information and quantum multipartite systems, quantum coherence is crucial for quantifying the inherent quantumness in the system. It can be rigorously defined within the framework of quantum resource theory and plays a vital role in numerous quantum information and estimation protocols. Additionally, it is primarily accountable for the superiority of quantum tasks over their classical counterparts. Beyond being a crucial element in quantum information processing, quantum coherence is also pivotal in emerging fields such as quantum metrology [44], nanoscale thermodynamics [45, 46], and quantum biology [47].

The coherence effect of a quantum state is typically attributed to the off-diagonal elements of its density matrix relative to a chosen reference basis, which is defined based on the specific physical problem at hand. While the theory of quantum coherence has long been established in the field of quantum optics, its quantification has gained significant attention only in recent years, driven by advancements in quantum information science. The first thorough framework for quantifying the coherence of quantum states within resource theories was established in the groundbreaking work of Ref. [48]. This work set forth stringent criteria for a quantity to qualify as a coherence measure. They also proposed the  $l_1$ -norm and the relative entropy of coherence, as two coherence measures which are based on rigorous metrics. This foundational study has since led to the development of numerous coherence measures tailored to different physical contexts, see for e.g., [49–58].

Furthermore, quantum coherence is intricately linked to various measures of quantum correlations, such as entanglement, quantum discord and non-locality, see for e.g., [59–64]. In particular, coherence and entanglement are inherently linked. It has been shown that nonzero coherence is both necessary and sufficient for a state to generate entanglement [62]. Additionally, under certain specific conditions, coherence and entanglement can be transformed into each other [61–64]. Thus, quantum coherence can be viewed as the foundational element that underpins almost all quantum correlations within the system. This fundamental relationship highlights the importance of coherence in the broader context of quantum mechanics and quantum information science.

In [65], quantum coherence, quantified using the  $l_1$ -norm, was examined in the context of three-flavor neutrino oscillations across various reactor and accelerator neutrino experiment setups. For these setups, the scale of quantum coherence—defined as the length over which coherence measures can maintain higher values—was identified. Ref. [66] explored quantum coherence in the context of neutrino spin-flavor oscillations (SFO) involving three-flavor mixing, considering both interstellar and intergalactic magnetic fields. The analysis employed the  $l_1$ -norm and relative entropy of coherence as quantifiers. Remarkably, the findings indicated that in the SFO scenario, quantum coherence could persist over incredibly vast astrophysical distances, spanning from kiloparsecs to gigaparsecs, suggesting that coherence is robust even across cosmic scales.

In this work, we present the first study of quantum coherence in flavor mode entangled neutrinos by conducting an extensive analysis of all relevant measures of quantum coherence in the context of three flavor neutrino oscillations by mapping the neutrino state as a three-

mode system to the tripartite basis of the one-qutrit and three-qubit system. For the sake of completeness, we also provide a detailed methodology for the coherence measures when the neutrino states (as two-mode systems) are mapped to the bipartite basis of the two-qubit system in the case of two-flavor mixing. Apart from the  $l_1$ -norm of coherence, we consider the relative entropy of coherence, robustness of coherence, coherence concurrence, trace-norm distance measure of coherence, coherence of formation, Schatten- $p$ -norm-based functionals, geometric coherence and the logarithmic coherence rank. It is important to note that, unlike the  $l_1$ -norm of coherence and the relative entropy of coherence, the other three measures are valid only for entangled systems.

The structure of this paper is organized as follows. In the next section, we present the methodology for modeling neutrinos as a qubit and qutrit systems, laying the groundwork for the analysis that follows. Sec. III presents the theoretical calculations of various quantum coherence measures for mode-entangled neutrinos, treating them as two- and three-qubit systems, as well as qutrits. Additionally, we map these theoretical expressions to plots that illustrate the dynamic behavior of these coherence measures. Finally, we provide our conclusions in Sec. IV.

## 2 Neutrinos as qubits and qutrit

The three flavor states of a neutrino— $\nu_e$ ,  $\nu_\mu$ , and  $\nu_\tau$ —with a specific handedness  $h$ , undergo oscillations within their flavor basis. These states are mixed through the unitary  $3 \times 3$  Pontecorvo–Maki–Nakagawa–Sakata (PMNS) leptonic mixing matrix  $U_{\alpha i}$ , resulting in a coherent superposition of the corresponding mass eigenstates  $\nu_1$ ,  $\nu_2$ , and  $\nu_3$ , all having the same handedness  $h$ , as expressed by

$$|\nu_\alpha^h(t)\rangle = \sum_{i=1}^3 U_{\alpha i} |\nu_i^h(t)\rangle = \sum_{i=1}^3 e^{-iE_i t} U_{\alpha i} |\nu_i^h(0)\rangle \quad \text{with} \quad U_{\alpha i} \in SU(3), \quad (2.1)$$

where the mass eigenstates of the neutrino evolve unitarily over time. Here,  $\alpha = e, \mu, \tau$ , and the PMNS matrix  $U_{\alpha i}$  is given by

$$U_{\alpha i} = \begin{pmatrix} c_{12}c_{13} & s_{12}c_{13} & s_{13} \\ -s_{12}c_{23} - c_{12}s_{23}s_{13} & c_{12}c_{23} - s_{12}s_{23}s_{13} & s_{23}c_{13} \\ s_{12}s_{23} - c_{12}c_{23}s_{13} & -c_{12}s_{23} - s_{12}c_{23}s_{13} & c_{23}c_{13} \end{pmatrix}, \quad (2.2)$$

where  $s_{ij} \equiv \sin \theta_{ij}$ ,  $c_{ij} \equiv \cos \theta_{ij}$  and  $\theta_{ij}$  represents the mixing angles  $\theta_{12}, \theta_{23}, \theta_{13}$ . It is seen that the mixing matrix is characterized by four degrees of freedom out of the nine possible for a three-dimensional unitary matrix, as the remaining five are absorbed as phases of the lepton fields. These four parameters include the three mixing angles  $\theta_{12}, \theta_{13}, \theta_{23}$  whose sines are  $\sin^2 \theta_{12} = 0.304$ ,  $\sin^2 \theta_{23} = 0.573$  and  $\sin^2 \theta_{13} = 0.022$  [67], and the complex charge-parity ( $CP$ ) violating phase  $\delta_{CP}$ , which we assume to be zero, thus neglecting the  $CP$ -violating effects.

In experimentally relevant scenarios, the complex three-flavor neutrino mixing can be simplified to an effective two-flavor mixing model using the  $SU(2)$  unitary rotation matrix.

This reduction is expressed as

$$\begin{pmatrix} |\nu_\alpha^h(t)\rangle \\ |\nu_\beta^h(t)\rangle \end{pmatrix} = \begin{pmatrix} \cos\theta & \sin\theta \\ -\sin\theta & \cos\theta \end{pmatrix} \begin{pmatrix} e^{-iE_i t} |\nu_i^h\rangle \\ e^{-iE_j t} |\nu_j^h\rangle \end{pmatrix}, \quad (2.3)$$

where  $\alpha$  and  $\beta$  are the flavor indices which can be  $e$ ,  $\mu$  or  $\tau$ , and  $i$  and  $j$  are the mass indices. Since in the case of two flavor mixing only one mixing angle between the two flavors is required, we denote the parameter simply by  $\theta$ . In the relativistic limit, the exact quantum field theoretic flavor states reduce to the more familiar Pontecorvo flavor states. These states are physically well-defined, representing distinct single-particle entities associated with specific flavor modes. Consequently, this framework allows us to define and analyze entanglement between these flavor modes, highlighting the quantum nature of neutrino oscillations.

The two-level ‘‘qubit’’ system is described by the two mutually orthogonal states

$$|0\rangle = \begin{pmatrix} 0 \\ 1 \end{pmatrix} \quad \text{and} \quad |1\rangle = \begin{pmatrix} 1 \\ 0 \end{pmatrix},$$

which exist within a complex two-dimensional Hilbert space  $\mathcal{H}^2$ . In this framework, we adopt the occupation number representation, where the presence of a single-particle state in a specific flavor mode (say  $\alpha$ ) is denoted by the qubit  $|1\rangle_\alpha$ , and its absence by  $|0\rangle_\alpha$ . Using this scheme, the flavor states at  $L = 0$  can be mapped to the bipartite basis states in a two-qubit system (for two-flavor mixing) as

$$|\nu_\alpha\rangle = |1\rangle_\alpha \otimes |0\rangle_\beta \quad \text{and} \quad |\nu_\beta\rangle = |0\rangle_\alpha \otimes |1\rangle_\beta.$$

Similarly, for three-flavor mixing, the flavor states at  $L = 0$  can be mapped to tripartite states in a three-qubit system as follows:

$$|\nu_e\rangle = |1\rangle_e \otimes |0\rangle_\mu \otimes |0\rangle_\tau, \quad |\nu_\mu\rangle = |0\rangle_e \otimes |1\rangle_\mu \otimes |0\rangle_\tau, \quad |\nu_\tau\rangle = |0\rangle_e \otimes |0\rangle_\mu \otimes |1\rangle_\tau.$$

This approach effectively captures the quantum states of neutrinos in terms of qubits, allowing for a clear representation of flavor mixing within two- and three-flavor systems.

Therefore, in the case of two-flavor mixing, the evolution of a single-particle mode-entangled neutrino flavor state, which starts in the flavor  $\alpha$  (where  $\alpha$  can be  $e$ ,  $\mu$ , or  $\tau$ ), can be described as a Bell-like superposition of two qubits in the Hilbert space  $\mathcal{H}^2 \otimes \mathcal{H}^2$  as

$$|\nu_\alpha(\theta, L)\rangle = \tilde{U}_{\alpha\alpha}(\theta, L)|1\rangle_\alpha \otimes |0\rangle_\beta + \tilde{U}_{\alpha\beta}(\theta, L)|0\rangle_\alpha \otimes |1\rangle_\beta, \quad (2.4)$$

where  $\alpha$  and  $\beta$  represent any two of the three available flavor modes:  $e$ ,  $\mu$ , or  $\tau$ . The coefficients of this Bell-like superposition, derived from the parameters governing neutrino flavor oscillations, are expressed as:

$$\begin{aligned} \tilde{U}_{\alpha\alpha}(\theta, L) &= \cos^2\theta e^{-iE_i L} + \sin^2\theta e^{-iE_j L}, \\ \tilde{U}_{\alpha\beta}(\theta, L) &= \cos\theta \sin\theta (e^{-iE_j L} - e^{-iE_i L}), \end{aligned} \quad (2.5)$$

where  $i, j = 1, 2, 3$  are the mass indices. The normalization condition is  $|\tilde{U}_{\alpha\alpha}(\theta, L)|^2 + |\tilde{U}_{\alpha\beta}(\theta, L)|^2 = 1$ , reflecting that  $|\tilde{U}_{\alpha\alpha}(\theta, L)|^2$  represents the survival probability of the flavor  $\alpha$ , while  $|\tilde{U}_{\alpha\beta}(\theta, L)|^2$  represents the probability of transition from the initial flavor  $\alpha$  to  $\beta$ .

Now from Eq. (2.4), the  $4 \times 4$  two-qubit density matrix  $\rho_{\alpha,2}^{4 \times 4}(\theta, L) = |\nu_\alpha(\theta, L)\rangle \langle \nu_\alpha(\theta, L)|$  for two neutrino flavor mixing can be written as<sup>1</sup>,

$$\rho_{\alpha,2}^{4 \times 4}(\theta, L) = \begin{pmatrix} 0 & 0 & 0 & 0 \\ 0 & |\tilde{U}_{\alpha\alpha}(\theta, L)|^2 & \tilde{U}_{\alpha\alpha}(\theta, L)\tilde{U}_{\alpha\beta}^*(\theta, L) & 0 \\ 0 & \tilde{U}_{\alpha\alpha}^*(\theta, L)\tilde{U}_{\alpha\beta}(\theta, L) & |\tilde{U}_{\alpha\beta}(\theta, L)|^2 & 0 \\ 0 & 0 & 0 & 0 \end{pmatrix}. \quad (2.6)$$

The time evolution of a mode-entangled neutrino flavor state in the three-flavor mixing scenario can be represented as a superposition of three qubits within the Hilbert space  $\mathcal{H}^2 \otimes \mathcal{H}^2 \otimes \mathcal{H}^2$  as<sup>2</sup>[5],

$$\begin{pmatrix} |\nu_e(\theta_{ij}, L)\rangle \\ |\nu_\mu(\theta_{ij}, L)\rangle \\ |\nu_\tau(\theta_{ij}, L)\rangle \end{pmatrix} = \begin{pmatrix} a_{ee}(\theta_{ij}, L) & a_{e\mu}(\theta_{ij}, L) & a_{e\tau}(\theta_{ij}, L) \\ a_{e\mu}(\theta_{ij}, L) & a_{\mu\mu}(\theta_{ij}, L) & a_{\mu\tau}(\theta_{ij}, L) \\ a_{e\tau}(\theta_{ij}, L) & a_{\mu\tau}(\theta_{ij}, L) & a_{\tau\tau}(\theta_{ij}, L) \end{pmatrix} \begin{pmatrix} |1\rangle \otimes |0\rangle \otimes |0\rangle \\ |0\rangle \otimes |1\rangle \otimes |0\rangle \\ |0\rangle \otimes |0\rangle \otimes |1\rangle \end{pmatrix}, \quad (2.7)$$

where the complex coefficients  $a_{\alpha\beta}(\theta_{ij}, L)$  with  $(\alpha, \beta) = e, \mu, \tau$  are given as,

$$\begin{aligned} a_{ee}(\theta_{ij}, L) &= c_{12}^2 c_{13}^2 e^{-iE_1 L} + s_{12}^2 c_{13}^2 e^{-iE_2 L} + s_{13}^2 e^{-iE_3 L}, \\ a_{\mu\mu}(\theta_{ij}, L) &= (s_{12} c_{23} + c_{12} s_{23} s_{13})^2 e^{-iE_1 L} + (c_{12} c_{23} - s_{12} s_{23} s_{13})^2 e^{-iE_2 L} + s_{23}^2 c_{13}^2 e^{-iE_3 L}, \\ a_{\tau\tau}(\theta_{ij}, L) &= (s_{12} s_{23} - c_{12} c_{23} s_{13})^2 e^{-iE_1 L} + (c_{12} s_{23} + s_{12} c_{23} s_{13})^2 e^{-iE_2 L} + c_{23}^2 c_{13}^2 e^{-iE_3 L}, \\ a_{e\mu}(\theta_{ij}, L) &= -(c_{12} c_{13} s_{12} c_{23} + c_{12}^2 c_{13} s_{23} s_{13}) e^{-iE_1 L} + (s_{12} c_{13} c_{12} c_{23} - s_{12}^2 c_{13} s_{23} s_{13}) e^{-iE_2 L} \\ &\quad + s_{13} s_{23} c_{13} e^{-iE_3 L}, \\ a_{e\tau}(\theta_{ij}, L) &= (c_{12} c_{13} s_{12} s_{23} - c_{12}^2 c_{13} c_{23} s_{13}) e^{-iE_1 L} - (s_{12} c_{13} c_{12} s_{23} + s_{12}^2 c_{13} c_{23} s_{13}) e^{-iE_2 L} \\ &\quad + s_{13} c_{23} c_{13} e^{-iE_3 L}, \\ a_{\mu\tau}(\theta_{ij}, L) &= (-s_{12}^2 c_{23} s_{23} + s_{12} c_{23}^2 c_{12} s_{13} - c_{12} s_{23}^2 s_{13} s_{12} + c_{12}^2 s_{23} s_{13}^2 c_{23}) e^{-iE_1 L} \\ &\quad + (-c_{12}^2 c_{23} s_{23} - c_{12} c_{23}^2 s_{12} s_{13} + s_{12} s_{23}^2 s_{13} c_{12} + s_{12}^2 c_{23} s_{13}^2 s_{23}) e^{-iE_2 L} \\ &\quad + s_{23} c_{13}^2 c_{23} e^{-iE_3 L}. \end{aligned} \quad (2.8)$$

The decompositions in Eq. (2.7) in the tripartite three-qubit basis gives us three  $8 \times 8$  three-qubit density matrices  $\rho_{\alpha,3}^{8 \times 8}(\theta_{ij}, L) = |\nu_\alpha(\theta_{ij}, L)\rangle \langle \nu_\alpha(\theta_{ij}, L)|$  for the three initial flavors

<sup>1</sup>The Dirac matrices which are tensor products of the Pauli matrices (that generate the SU(2) group)  $D_{\mu\nu} = \sigma_\mu \otimes \sigma_\nu$  serve as the basis for constructing these  $4 \times 4$  density matrices.

<sup>2</sup>We get this symmetric transformation matrix due to the fact that we consider negligible  $CP$ -violating phase in the mixing matrix, and hence all the PMNS matrix elements are considered to be real, which results in the coefficients in Eq. (2.8) being symmetric in the two indices  $\alpha, \beta$ .

$\alpha = e, \mu, \tau$  as,

$$\rho_{\alpha,3}^{8 \times 8}(\theta_{ij}, L) = \begin{pmatrix} 0 & 0 & 0 & 0 & 0 & 0 & 0 & 0 \\ 0 & |a_{\alpha\tau}(\theta_{ij}, L)|^2 & a_{\alpha\tau}^*(\theta_{ij}, L) a_{\alpha\mu}(\theta_{ij}, L) & 0 & a_{\alpha\tau}^*(\theta_{ij}, L) a_{\alpha e}(\theta_{ij}, L) & 0 & 0 & 0 \\ 0 & a_{\alpha\mu}^*(\theta_{ij}, L) a_{\alpha\tau}(\theta_{ij}, L) & |a_{\alpha\mu}(\theta_{ij}, L)|^2 & 0 & a_{\alpha\mu}^*(\theta_{ij}, L) a_{\alpha e}(\theta_{ij}, L) & 0 & 0 & 0 \\ 0 & 0 & 0 & 0 & 0 & 0 & 0 & 0 \\ 0 & a_{\alpha e}^*(\theta_{ij}, L) a_{\alpha\tau}(\theta_{ij}, L) & a_{\alpha e}^*(\theta_{ij}, L) a_{\alpha\mu}(\theta_{ij}, L) & 0 & |a_{\alpha e}(\theta_{ij}, L)|^2 & 0 & 0 & 0 \\ 0 & 0 & 0 & 0 & 0 & 0 & 0 & 0 \\ 0 & 0 & 0 & 0 & 0 & 0 & 0 & 0 \\ 0 & 0 & 0 & 0 & 0 & 0 & 0 & 0 \end{pmatrix}. \quad (2.9)$$

As demonstrated in [68], entangled qutrits are less susceptible to noise compared to entangled qubits and can achieve maximal violation of Bell's inequality. With this in mind, we shift our focus from the two-level qubit system to a more general three-level quantum system known as the ‘‘qutrit.’’ This system is spanned by three mutually orthogonal states

$$|1\rangle = \begin{pmatrix} 1 \\ 0 \\ 0 \end{pmatrix}, \quad |2\rangle = \begin{pmatrix} 0 \\ 1 \\ 0 \end{pmatrix}, \quad |3\rangle = \begin{pmatrix} 0 \\ 0 \\ 1 \end{pmatrix},$$

residing in a complex three-dimensional Hilbert space  $\mathcal{H}^3$ . In this framework, the initial flavor states at  $L = 0$  can be mapped to the basis states of the one-qutrit system (for three-flavor mixing) as  $|\nu_e\rangle = |1\rangle$ ,  $|\nu_\mu\rangle = |2\rangle$ , and  $|\nu_\tau\rangle = |3\rangle$ . The three-flavor evolution of mode-entangled neutrinos can then be described as a superposition of qutrits in  $\mathcal{H}^3$ , as discussed in [10],

$$\begin{pmatrix} |\nu_e(\theta_{ij}, L)\rangle \\ |\nu_\mu(\theta_{ij}, L)\rangle \\ |\nu_\tau(\theta_{ij}, L)\rangle \end{pmatrix} = \begin{pmatrix} c_{12}c_{13} & -s_{12}c_{23} - c_{12}s_{23}s_{13} & s_{12}s_{23} - c_{12}c_{23}s_{13} \\ s_{12}c_{13} & c_{12}c_{23} - s_{12}s_{23}s_{13} & -c_{12}s_{23} - s_{12}c_{23}s_{13} \\ s_{13} & s_{23}c_{13} & c_{23}c_{13} \end{pmatrix} \begin{pmatrix} e^{-iE_1 L}|1\rangle \\ e^{-iE_2 L}|2\rangle \\ e^{-iE_3 L}|3\rangle \end{pmatrix}, \quad (2.10)$$

We can immediately identify the transformation matrix in the above equation as the transpose of the PMNS matrix with the complex  $CP$ -violating phase assumed to be zero. From Eq. (2.10), we can then get the three hermitian  $3 \times 3$  one-qutrit density matrices  $\rho_{e,3}^{3 \times 3}(\theta_{ij}, L) = |\nu_e(\theta_{ij}, L)\rangle \langle \nu_e(\theta_{ij}, L)|$ ,  $\rho_{\mu,3}^{3 \times 3}(\theta_{ij}, L) = |\nu_\mu(\theta_{ij}, L)\rangle \langle \nu_\mu(\theta_{ij}, L)|$  and  $\rho_{\tau,3}^{3 \times 3}(\theta_{ij}, L) = |\nu_\tau(\theta_{ij}, L)\rangle \langle \nu_\tau(\theta_{ij}, L)|$  as<sup>3</sup>,

$$\rho_{e,3}^{3 \times 3}(\theta_{ij}, L) = \begin{pmatrix} c_{12}^2 c_{13}^2 & \hat{\rho}_{e,12}(\theta_{ij}) e^{i \frac{\Delta m_{21}^2}{2E} L} & \hat{\rho}_{e,13}(\theta_{ij}) e^{i \frac{\Delta m_{31}^2}{2E} L} \\ \hat{\rho}_{e,12}(\theta_{ij}) e^{-i \frac{\Delta m_{21}^2}{2E} L} & (s_{12}c_{13} + c_{12}s_{23}s_{13})^2 & \hat{\rho}_{e,23}(\theta_{ij}) e^{i \frac{\Delta m_{32}^2}{2E} L} \\ \hat{\rho}_{e,13}(\theta_{ij}) e^{-i \frac{\Delta m_{31}^2}{2E} L} & \hat{\rho}_{e,23}(\theta_{ij}) e^{-i \frac{\Delta m_{32}^2}{2E} L} & (s_{12}s_{23} - c_{12}c_{23}s_{13})^2 \end{pmatrix}, \quad (2.11)$$

$$\rho_{\mu,3}^{3 \times 3}(\theta_{ij}, L) = \begin{pmatrix} s_{12}^2 c_{13}^2 & \hat{\rho}_{\mu,12}(\theta_{ij}) e^{i \frac{\Delta m_{21}^2}{2E} L} & \hat{\rho}_{\mu,13}(\theta_{ij}) e^{i \frac{\Delta m_{31}^2}{2E} L} \\ \hat{\rho}_{\mu,12}(\theta_{ij}) e^{-i \frac{\Delta m_{21}^2}{2E} L} & (c_{12}c_{13} - s_{12}s_{23}s_{13})^2 & \hat{\rho}_{\mu,23}(\theta_{ij}) e^{i \frac{\Delta m_{32}^2}{2E} L} \\ \hat{\rho}_{\mu,13}(\theta_{ij}) e^{-i \frac{\Delta m_{31}^2}{2E} L} & \hat{\rho}_{\mu,23}(\theta_{ij}) e^{-i \frac{\Delta m_{32}^2}{2E} L} & (c_{12}s_{23} + s_{12}c_{23}s_{13})^2 \end{pmatrix}, \quad (2.12)$$

<sup>3</sup>These  $3 \times 3$  density matrices are constructed using the Gell-Mann matrices (generators of the SU(3) group) as basis.

$$\rho_{\tau,3}^{3 \times 3}(\theta_{ij}, L) = \begin{pmatrix} s_{13}^2 & s_{13}c_{13}s_{23}e^{i\frac{\Delta m_{21}^2}{2E}L} & s_{13}c_{13}c_{23}e^{i\frac{\Delta m_{31}^2}{2E}L} \\ s_{13}c_{13}s_{23}e^{-i\frac{\Delta m_{21}^2}{2E}L} & c_{13}^2s_{23}^2 & s_{23}c_{23}c_{13}^2e^{i\frac{\Delta m_{32}^2}{2E}L} \\ s_{13}c_{13}c_{23}e^{-i\frac{\Delta m_{31}^2}{2E}L} & s_{23}c_{23}c_{13}^2e^{-i\frac{\Delta m_{32}^2}{2E}L} & c_{13}^2c_{23}^2 \end{pmatrix}, \quad (2.13)$$

where the neutrino energy difference in the phase factors are given by<sup>4</sup>

$$E_i - E_j = \begin{cases} \frac{\Delta m_{ij}^2}{2E} & \text{for } i > j \\ -\frac{\Delta m_{ji}^2}{2E} & \text{for } i < j \end{cases}.$$

The real-valued off-diagonal elements in the density matrix in Eq. (2.11) are given as functions of the mixing angles  $\theta_{ij}$  as,

$$\begin{aligned} \hat{\rho}_{e,12}(\theta_{ij}) &= -s_{12}c_{23}c_{12}c_{13} - c_{12}^2c_{13}s_{23}s_{13}, \\ \hat{\rho}_{e,13}(\theta_{ij}) &= s_{12}s_{23}c_{12}c_{13} - c_{12}^2c_{13}c_{23}s_{13}, \\ \hat{\rho}_{e,23}(\theta_{ij}) &= -s_{12}^2c_{23}s_{23} + s_{12}c_{12}c_{23}^2s_{13} - c_{12}s_{23}^2s_{13}s_{12} + c_{12}^2s_{23}c_{23}s_{13}^2, \end{aligned} \quad (2.14)$$

and the off-diagonal elements in (2.12) are given as,

$$\begin{aligned} \hat{\rho}_{\mu,12}(\theta_{ij}) &= s_{12}c_{12}c_{13}c_{23} - s_{12}^2c_{13}s_{23}s_{13}, \\ \hat{\rho}_{\mu,13}(\theta_{ij}) &= -s_{12}s_{23}c_{12}c_{13} - s_{12}^2c_{13}c_{23}s_{13}, \\ \hat{\rho}_{\mu,23}(\theta_{ij}) &= -c_{12}^2c_{23}s_{23} - s_{12}c_{12}c_{23}^2s_{13} + c_{12}s_{23}^2s_{13}s_{12} + s_{12}^2s_{23}c_{23}s_{13}^2. \end{aligned} \quad (2.15)$$

We are now equipped with all the density matrices required for the calculation of various coherence measures in both the two-flavor and three-flavor mixing scenarios.

### 3 Measures of quantum coherence

A completely positive and trace preserving (CPTP) U(1)-covariant incoherent operation can be expressed as a function of the density operator  $\rho$  as,

$$\Xi_{\text{ICPTP}}(\rho) = \sum_{\ell} K_{\ell} \rho K_{\ell}^{\dagger}, \quad (3.1)$$

where  $K_{\ell}$  represents the incoherent Kraus operators that satisfy  $\sum_{\ell} K_{\ell}^{\dagger} K_{\ell} = \mathbb{1}$  and  $\ell$  represents individual outcomes corresponding to which the states are given by  $\rho_{\ell} = \frac{K_{\ell} \rho K_{\ell}^{\dagger}}{p_{\ell}}$  where the probability of occurrence of such a state is given by  $p_{\ell} = \text{Tr}(K_{\ell} \rho K_{\ell}^{\dagger})$ . The Kraus operators transform any incoherent state into another incoherent state fulfilling  $K_{\ell} \mathcal{I} K_{\ell}^{\dagger} \subset \mathcal{I} \forall \ell$ , with  $\mathcal{I}$  representing the set of incoherent quantum states which can be expressed as pure state decomposition  $\sum_{i=1}^d \sigma_i |i\rangle \langle i|$  with probability of occurrence being  $|\sigma_i|^2$ , where the Hilbert space  $\mathcal{H}^d$  is d-dimensional. So the states diagonal in the reference

<sup>4</sup>The neutrino mass-squared splitting parameters are  $\Delta m_{21}^2 = 7.42 \times 10^{-5} \text{ eV}^2$  and  $|\Delta m_{32}|^2 \simeq |\Delta m_{31}|^2 = 2.51 \times 10^{-3} \text{ eV}^2$  as per the constraints imposed by the current global fits [67].

basis  $\{|i\rangle\}_{i=1,2,\dots,n}$  are incoherent, and the states that cannot be expressed in this form are termed coherent. Coherence can be mathematically depicted as a functional of density operators  $C(\rho)$  that maps the states to non-negative real numbers. This mapping has to satisfy some conditions for the measure of coherence to be called “proper”.

The first condition ( $\mathbf{C}_1$ ) is *Faithfulness*, which asserts that  $C(\rho) \geq 0$  for any quantum state  $\rho$ , and specifically,  $C(\rho)$  should vanish for incoherent states. In other words,  $C(\sigma) = 0$  if and only if  $\sigma \in \mathcal{I}$ , meaning that  $\sigma$  is an incoherent state. This condition is crucial because it ensures that the coherence measure accurately distinguishes between coherent and incoherent states. This condition is also often referred to as the “Non-negativity” condition, reflecting its requirement that the measure be non-negative for all states.

The second condition is *Monotonicity* ( $\mathbf{C}_2$ ), which requires that the coherence measure  $C(\rho)$  should not increase under incoherent completely positive and trace-preserving (CPTP) maps. Mathematically, this is expressed as  $C(\Xi_{\text{ICPTP}}(\rho)) \leq C(\rho)$  for all incoherent operations  $\Xi_{\text{ICPTP}}$ . This condition ensures that coherence, as a resource, cannot be generated for free through operations that are deemed incoherent. However, this condition does not account for scenarios where the measurement outcomes are retained. To capture these scenarios, a stronger condition, known as *Strong Monotonicity* ( $\mathbf{C}'_2$ ), is imposed. This condition requires that  $C(\rho) \geq \sum_{\ell} p_{\ell} C(\rho_{\ell})$  for all sets of Kraus operators  $\{K_{\ell}\}$ , ensuring that the expected coherence does not increase even when the measurement results are known. This stronger requirement is vital, as it rules out certain measures, such as those based on fidelity, from being considered proper measures of coherence since they do not generally satisfy  $\mathbf{C}'_2$ <sup>5</sup>.

The final essential condition on  $C(\rho)$  is *Convexity* ( $\mathbf{C}_3$ ), which stipulates that the coherence measure should not increase under the mixing of quantum states. Specifically, for any set of states  $\{\rho_{\ell}\}$  and probabilities  $p_{\ell} \geq 0$  with  $\sum_{\ell} p_{\ell} = 1$ , the condition requires that  $C(\sum_{\ell} p_{\ell} \rho_{\ell}) \leq \sum_{\ell} p_{\ell} C(\rho_{\ell})$ . This condition is important because it prevents artificial increases in coherence due to probabilistic mixtures of states, thereby ensuring that the measure respects the notion that mixing cannot generate coherence.

We will now explore ten potential coherence monotones within the context of two- and three-flavor mode-entangled neutrino oscillations. In these cases, the neutrino states are mapped onto two-qubit systems for two-flavor mixing and three-qubit as well as one-qutrit systems for three-flavor mixing. We will express these monotones in terms of measurable parameters associated with neutrino oscillations.

### 3.1 $l_1$ -norm of coherence

If  $\mathcal{V}^{m \times n}$  is a vector space with  $m \times n$  matrices, then the  $l_p$  norm on  $\mathcal{V}^{m \times n}$  induced by the vector  $p$ -norms for both the vector spaces  $\mathcal{V}^m$  and  $\mathcal{V}^n$  can be given as  $\left(\sum_{m \neq n} |\rho_{mn}|^p\right)^{\frac{1}{p}}$ , where  $\rho_{mn} = \langle m | \rho | n \rangle$  are the matrix elements. For  $p = 1$ , the  $l_{p=1}$  matrix norm satisfies all the conditions  $\mathbf{C}_1$ ,  $\mathbf{C}_2$ ,  $\mathbf{C}'_2$  and  $\mathbf{C}_3$  for being a proper measure of coherence, and clasps the sum of the absolute magnitudes of all off-diagonal entries in the density matrix  $\rho(t)$

---

<sup>5</sup>This condition is crucial for ruling out measures of coherence induced by the fidelity between two quantum states as proper coherence measures, as they do not generally satisfy  $\mathbf{C}'_2$  [51].

and can take a maximum value of  $r - 1$ , where  $r$  represents the dimension of  $\rho(t)$ . Hence, as a function of  $\rho(t)$ , the  $l_1$ -norm of coherence is given as,

$$C_{l_1}(\rho) \equiv \sum_{m \neq n} |\langle m | \rho(t) | n \rangle| \geq 0. \quad (3.2)$$

Now let us first consider the effective two-flavor mixing scenario, where we map the initial neutrino flavor states to the bipartite basis states in the two-qubit coupled system represented by the  $4 \times 4$  density matrix  $\rho_{\alpha,2}^{4 \times 4}(\theta, L)$  in Eq. (2.6) using which, the  $l_1$ -norm of coherence can be expressed through the definition in Eq. (3.2) as

$$C_{l_1}^{2f}(\rho_{\alpha,2}^{4 \times 4}) = \sum_{m \neq n} |\langle m | \rho_{\alpha,2}^{4 \times 4}(\theta, L) | n \rangle| = |\tilde{U}_{\alpha\alpha}(\theta, L)\tilde{U}_{\alpha\beta}^*(\theta, L)| + |\tilde{U}_{\alpha\alpha}^*(\theta, L)\tilde{U}_{\alpha\beta}(\theta, L)|. \quad (3.3)$$

Now we can use the coefficients from Eq. (2.5) in the above equation, which gives us,

$$\begin{aligned} C_{l_1}^{2f}(\rho_{\alpha,2}^{4 \times 4}) &= \{ |(\cos^2 \theta e^{-iE_i L} + \sin^2 \theta e^{-iE_j L}) \sin \theta \cos \theta (e^{iE_j t} - e^{iE_i t})| \\ &\quad + |(\cos^2 \theta e^{iE_i t} + \sin^2 \theta e^{iE_j t}) \sin \theta \cos \theta (e^{-iE_j L} - e^{-iE_i L})| \} \\ &= 2|\sin \theta \cos \theta| |e^{iE_j t} - e^{iE_i t}| |\cos^2 \theta e^{iE_i t} + \sin^2 \theta e^{iE_j t}|. \end{aligned} \quad (3.4)$$

On simplification, we arrive at

$$\begin{aligned} C_{l_1}^{2f}(\rho_{\alpha,2}^{4 \times 4}) &= |\sin 2\theta| \sqrt{2 \left( 1 - \cos \frac{\Delta m_{ij}^2 t}{2p} \right) \sin^2 \theta \cos^2 \theta \left( \cot^2 \theta + \tan^2 \theta + 2 \cos \frac{\Delta m_{ij}^2 t}{2p} \right)} \\ &= \frac{\sin^2 2\theta}{\sqrt{2}} \sqrt{\cot^2 \theta + \tan^2 \theta - 2 \cos^2 \frac{\Delta m_{ij}^2 t}{2p} - (\cot \theta - \tan \theta)^2 \cos \frac{\Delta m_{ij}^2 t}{2p}}, \end{aligned} \quad (3.5)$$

where in the final step, we used the relationship  $E_i - E_j = \frac{\Delta m_{ij}^2}{2p}$  for  $i > j$ , where  $E_i$  and  $E_j$  are the energy eigenvalues corresponding to the mass eigenstates  $\nu_i$  and  $\nu_j$ , respectively. This relationship is crucial for expressing the phase differences in terms of the mass-squared differences  $\Delta m_{ij}^2$ , which are key measurable parameters in neutrino oscillation experiments. The mixing angle  $\theta$  between the two states  $i$  and  $j$  (where  $i, j = 1, 2, 3$ ) is denoted simply as  $\theta$ , and it can correspond to any of the mixing angles  $\theta_{12}$ ,  $\theta_{23}$ , or  $\theta_{13}$  depending on the specific flavors involved in the mixing. This notation is consistent with the previous sections, where we used  $\theta$  to describe the mixing between different flavor states. For the two-flavor mixing scenario, we will continue using this  $\theta$ -notation for the calculation of the remaining coherence measures, ensuring consistency and clarity throughout the analysis.

In the standard prescription of two-flavor oscillations, the density matrix is a  $2 \times 2$  matrix, which constrains the maximum value of the  $l_1$ -norm of coherence to be 1. However, when entanglement between flavor modes is considered, the  $l_1$ -norm of coherence can exceed the standard maximum of 1. This enhancement arises from the additional degrees of freedom present in the two-qubit system, represented by a  $4 \times 4$  density matrix, which allows for more complex coherence dynamics compared to the simpler two-dimensional case.

For the three-flavor mixing scenario, where the neutrino states are mapped to the one-qutrit basis, we can apply a similar approach as in the two-flavor case, focusing on the flavor evolution of the mode-entangled electron (or muon) neutrino state  $|\nu_{e(\mu)}(\theta_{ij}, L)\rangle$ . By utilizing the  $3 \times 3$  density matrix  $\rho_{e(\mu),3}^{3 \times 3}(\theta_{ij}, L)$  from Eq. (2.11) (and Eq. (2.12)), we can compute the  $l_1$ -norm of coherence as follows:

$$\begin{aligned} C_{l_1}^{3f} \left( \rho_{e(\mu),3}^{3 \times 3} \right) &= \sum_{m \neq n} |\langle m | \rho_{e(\mu),3}^{3 \times 3}(\theta_{ij}, L) | n \rangle| \\ &= \sum_{j>i=1}^3 \left( |\hat{\rho}_{e(\mu),ij} e^{-i \frac{\Delta m_{ji}^2}{2p} t}| + |\hat{\rho}_{e(\mu),ij} e^{i \frac{\Delta m_{ji}^2}{2p} t}| \right) = 2 \sum_{j>i=1}^3 |\hat{\rho}_{e(\mu),ij}|, \end{aligned} \quad (3.6)$$

where the matrix elements  $\hat{\rho}_{e,ij}$  can be obtained from Eq. (2.14), allowing us to express  $C_{l_1}^{3f} \left( \rho_{e,3}^{3 \times 3} \right)$  in terms of measurable parameters as follows:

$$\begin{aligned} C_{l_1}^{3f} \left( \rho_{e,3}^{3 \times 3} \right) &= 2 \{ |s_{12}c_{23}c_{12}c_{13} + c_{12}^2c_{13}s_{23}s_{13}| + |s_{12}s_{23}c_{12}c_{13} - c_{12}^2c_{13}c_{23}s_{13}| \\ &\quad + | -s_{12}^2c_{23}s_{23} + s_{12}c_{12}c_{23}^2s_{13} - c_{12}s_{23}^2s_{13}s_{12} + c_{12}^2s_{23}c_{23}s_{13}^2| \}, \end{aligned} \quad (3.7)$$

and the matrix elements  $\hat{\rho}_{\mu,ij}$  can be obtained from Eq. (2.15), allowing us to express  $C_{l_1}^{3f} \left( \rho_{\mu,3}^{3 \times 3} \right)$  in terms of measurable parameters as follows:

$$\begin{aligned} C_{l_1}^{3f} \left( \rho_{\mu,3}^{3 \times 3} \right) &= 2 \{ |s_{12}c_{12}c_{13}c_{23} - s_{12}^2c_{13}s_{23}s_{13}| + |s_{12}s_{23}c_{12}c_{13} + s_{12}^2c_{13}c_{23}s_{13}| \\ &\quad + | -c_{12}^2c_{23}s_{23} - s_{12}c_{12}c_{23}^2s_{13} + c_{12}s_{23}^2s_{13}s_{12} + s_{12}^2s_{23}c_{23}s_{13}^2| \} \end{aligned} \quad (3.8)$$

In the one-qutrit mapping scenario, a notable distinction compared to the two-qubit case (for two-flavor mixing) is that the coherence measure  $C_{l_1}^{3f} \left( \rho_{\mu,3}^{3 \times 3} \right)$  stabilizes at a constant value of 1.95, while  $C_{l_1}^{3f} \left( \rho_{e,3}^{3 \times 3} \right)$  stabilizes at 1.62 for mode-entangled oscillations. The values of all coherence measures for the qutrit framework for both initial  $\nu_e$  and  $\nu_\mu$  initial states are represented in Fig. 2 wherein the  $l_1$ -norm of coherence is given in the top-left panel. This constancy is primarily because, in Eq. (3.6), the expression for  $C_{l_1}^{3f} \left( \rho_{e(\mu),3}^{3 \times 3} \right)$  lacks any dependence on the neutrino energy  $E$  or the distance  $L$  traversed by the neutrino. In the ultra-relativistic limit, where  $t \approx L$ , the coherence measure is determined solely by the fixed mixing angles, represented by sine and cosine terms (i.e.,  $s_{ij}$  and  $c_{ij}$ ). These terms combine through the matrix elements  $\hat{\rho}_{e,ij}$  as defined in Eqs. (2.14) and (2.15), leading to a constant value. In contrast, the two-flavor mixing case, represented by  $C_{l_1}^{2f} \left( \rho_{\alpha,2}^{4 \times 4} \right)$ , displays oscillatory behavior. This oscillation arises due to the explicit presence of the neutrino oscillation phase  $\frac{\Delta m_{ij}^2}{2p} t$ , which introduces energy and distance dependence into the coherence measure. The differences in behavior between the two-qubit and one-qutrit systems highlight the unique dynamics of quantum coherence in different neutrino mixing scenarios, emphasizing the impact of dimensionality and the specific mixing parameters on the evolution of coherence.

When we map the neutrino states to the tripartite three-qubit basis, considering the three-flavor evolution of the mode entangled neutrino  $|\nu_\alpha(\theta_{ij}, L)\rangle$  of an initial flavor  $\alpha$ , we

use the  $8 \times 8$  density matrices  $\rho_{\alpha,3}^{8 \times 8}(\theta_{ij}, L)$  from Eq. (2.9) and get the  $l_1$ -norm of coherence as,

$$C_{l_1}^{3f}(\rho_{\alpha,3}^{8 \times 8}) = \sum_{m \neq n} |\langle m | \rho_{\alpha,3}^{8 \times 8}(\theta_{ij}, L) | n \rangle| = \frac{1}{2} \sum_{(\beta \neq \gamma)=e}^{\tau} \left( |a_{\alpha\beta}^*(\theta_{ij}, L) a_{\alpha\gamma}(\theta_{ij}, L)| + |a_{\alpha\beta}(\theta_{ij}, L) a_{\alpha\gamma}^*(\theta_{ij}, L)| \right) = \sum_{(\beta \neq \gamma)=e}^{\tau} |a_{\alpha\beta}^*(\theta_{ij}, L) a_{\alpha\gamma}(\theta_{ij}, L)|, \quad (3.9)$$

where the complex coefficients  $a_{\alpha(e,\mu,\tau)}(\theta_{ij}, L)$  from Eq. (2.8) can be put into Eq. (3.9) to express  $C_{l_1}^{3f}(\rho_{\alpha,3}^{8 \times 8})$  in terms of the measurable neutrino oscillation parameters. In Eq. (3.9), we essentially calculate the sum of six off-diagonal matrix elements, selected from the nine non-zero elements in the  $8 \times 8$  three-qubit density matrices, as depicted in Eq. (2.9). The  $l_1$ -norm of coherence considering the initial neutrino flavor  $\alpha = e$ , i.e.  $C_{l_1}^{3f}(\rho_{e,3}^{8 \times 8})$  can be expressed in terms of the measurable parameters as,

$$C_{l_1}^{3f}(\rho_{e,3}^{8 \times 8}) = 2 \left\{ |a_{ee}^*(\theta_{ij}, L) a_{e\mu}(\theta_{ij}, L)| + |a_{ee}^*(\theta_{ij}, L) a_{e\tau}(\theta_{ij}, L)| + |a_{e\mu}^*(\theta_{ij}, L) a_{e\tau}(\theta_{ij}, L)| \right\}, \quad (3.10)$$

where the product of coefficients  $a_{e\beta}(\theta_{ij}, L)$  appearing in above equation have been evaluated in the first three equations in Appendix A.1.

The  $l_1$ -norm of coherence considering the initial neutrino flavor  $\alpha = \mu$ , i.e.  $C_{l_1}^{3f}(\rho_{\mu,3}^{8 \times 8})$  can be expressed in terms of the measurable parameters as,

$$C_{l_1}^{3f}(\rho_{\mu,3}^{8 \times 8}) = 2 \left\{ |a_{e\mu}^*(\theta_{ij}, L) a_{\mu\mu}(\theta_{ij}, L)| + |a_{e\mu}^*(\theta_{ij}, L) a_{\mu\tau}(\theta_{ij}, L)| + |a_{\mu\mu}^*(\theta_{ij}, L) a_{\mu\tau}(\theta_{ij}, L)| \right\}, \quad (3.11)$$

where the product of coefficients  $a_{\mu\beta}(\theta_{ij}, L)$  appearing in above equation are detailed in the last three equations in Appendix A.1.

Contrary to the scenario where neutrino states are mapped to the one-qutrit basis for three-flavor mixing, the  $l_1$  norm of coherence in the three-qubit framework shows a dependency on the distance traveled  $L$  and neutrino energy  $E$ . The  $l_1$  norm of coherence,  $C_{l_1}^{3f}(\rho_{\alpha,3}^{8 \times 8})$ , for  $\alpha = e, \mu$  evolves with neutrino propagation and is plotted as a function of  $\phi = \frac{\Delta m_{21}^2 L}{4E}$  in Fig. 1. For this measure, as well as for all other measures considered in this work, we present plots only for the dynamical behavior of metrics in the context of three-flavor oscillations.

The plot clearly demonstrates an inverse relationship between the dynamics of the  $l_1$ -norm of coherence and the survival probability  $P(\nu_\alpha \rightarrow \nu_\alpha)$ , where  $\alpha$  represents either the electron or muon flavor. Notably, when the  $l_1$ -norm reaches its peak value, the survival probability  $P_{\alpha\alpha}$  is at its minimum. For both the initial electron-neutrino and muon-neutrino cases, this occurs at  $\phi = \pi/2$ . This observation implies a strong correlation between the coherence measure and the oscillation rate of the neutrino flavors. A large value of the  $l_1$  norm suggests that the neutrinos are in a superposition state with a strong quantum

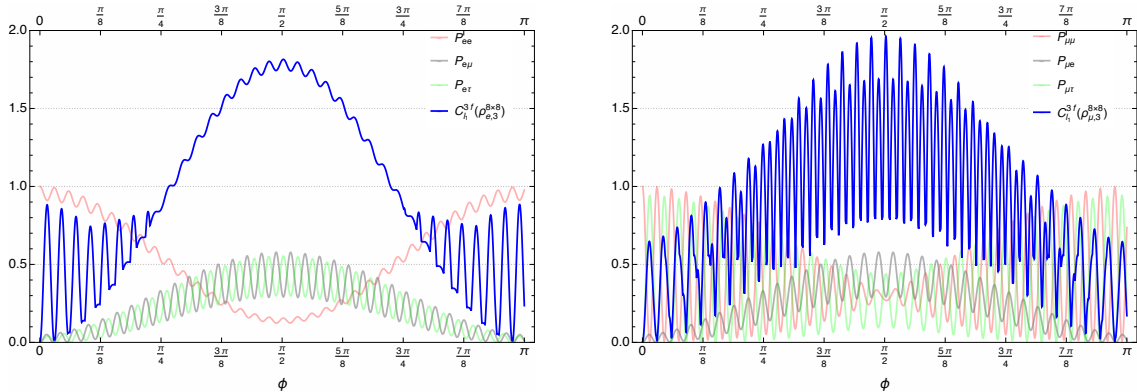


**Figure 1.** The figure illustrates the  $l_1$  norm of coherence,  $C_{l_1}^{3f}(\rho_{\mu,3}^{8\times 8})$  (right panel) and  $C_{l_1}^{3f}(\rho_{e,3}^{8\times 8})$  (left panel), along with the corresponding survival probability  $\nu_\mu \rightarrow \nu_\mu$  and transition probabilities  $\nu_\mu \rightarrow \nu_e$  and  $\nu_\mu \rightarrow \nu_\tau$  (right panel), as well as the probabilities  $\nu_e \rightarrow \nu_e$ ,  $\nu_e \rightarrow \nu_\mu$ , and  $\nu_e \rightarrow \nu_\tau$  (left panel). These quantities are plotted as functions of  $\phi$  which is defined as  $\phi = \frac{\Delta m_{21}^2 L}{4E}$ , for both the initial muon-neutrino (right-panel) and electron-neutrino states (left-panel). The analysis is performed within the framework of three-flavor neutrino oscillations, where the neutrino state is modelled as a three-mode system and mapped onto the tripartite basis of a three-qubit system.

correlation between different flavors. A high  $l_1$ -norm corresponds to a rapid oscillation between different flavors, resulting in a reduced survival probability for the initial muon neutrino state. Conversely, as the  $l_1$ -norm decreases, the survival probability increases, reflecting a slower oscillation rate and a higher chance that the electron or muon neutrino retains its original flavor state.

Additionally, the plots show that the  $l_1$ -norm of coherence remains non-zero throughout the entire oscillation cycle, even during phases where the oscillation rate is minimal. This indicates that the neutrino system retains a significant amount of quantum coherence across the entire range of the phase  $\phi$ . The persistence of non-zero coherence highlights the continuous presence of quantum correlations within the system. When comparing the initial electron-neutrino and muon-neutrino cases, a subtle difference is noticeable: the overall value of coherence is marginally higher for the muon-neutrino state. This slight increase suggests that the muon-neutrino state exhibits a stronger degree of coherence during oscillations. This may be attributed to the specific mixing angles and mass-squared differences that govern the dynamics of the muon-neutrino, which could lead to more pronounced quantum correlations within the system.

When comparing the peak values of  $C_{l_1}^{3f}(\rho_{e,3}^{3\times 3})$  and  $C_{l_1}^{3f}(\rho_{\mu,3}^{3\times 3})$ , which are around 1.62 and 1.95, respectively, with those in the one-qutrit framework, it becomes evident that the values obtained within the three-qubit framework are slightly higher for both initial  $\nu_e$  and  $\nu_\mu$  states. This marginal increase in coherence in the three-qubit system can be attributed to the dimensionality and structure of the quantum system.

**Robustness of coherence:** The robustness of coherence  $C_R(\rho)$  is another important measure for quantifying coherence in quantum systems. This measure is defined within the convex set of density operators  $\mathcal{D}(\mathbb{C}^d)$ , which act on a  $d$ -dimensional Hilbert space, as

detailed in [69]. Mathematically, it is expressed as:

$$C_R(\rho) = \min_{\tau \in \mathcal{D}(\mathbb{C}^d)} \left\{ s \geq 0 \left| \frac{\rho + s\tau}{1+s} =: \delta \in \mathcal{I} \right. \right\} \quad (3.12)$$

This equation defines the robustness of coherence as the minimal weight  $s$  of another arbitrary quantum state  $\tau$  that, when mixed convexly with the state  $\rho$ , produces an incoherent state  $\delta$  belonging to the set of incoherent states  $\mathcal{I}$ . In essence, this measure quantifies the smallest amount of "noise" or additional state  $\tau$  required to make the quantum state  $\rho$  indistinguishable from an incoherent state. The robustness of coherence, therefore, provides a clear operational meaning: it measures the resilience of quantum coherence against the introduction of external disturbances. This resilience is particularly relevant in practical scenarios where the integrity of quantum coherence is crucial, such as in quantum computation, quantum communication, and other quantum information processing tasks. By understanding the robustness of coherence, one can gauge how much external noise a quantum system can tolerate before losing its coherence, thereby offering insights into the stability and reliability of the quantum states under various conditions.

This measure is particularly useful because it can also be characterized by linear inequalities in the case of a  $d$ -dimensional quantum system, as shown in [70]. Specifically, the robustness of coherence satisfies the following bounds:

$$\frac{C_{l_1}(\rho)}{d-1} \geq C_R(\rho) \geq C_{l_1}(\rho), \quad (3.13)$$

where both the upper and lower bounds are quite tight. Notably, the upper bound becomes an equality, i.e.,  $C_R(\rho) = C_{l_1}(\rho)$ , for pure states. This equality is particularly relevant for the neutrino mode-entangled systems under consideration, where the robustness of coherence simplifies to the  $l_1$ -norm of coherence, thereby offering a straightforward method for analyzing coherence in these systems.

**Trace-norm distance measure of coherence:** A measure of coherence induced by the trace-norm distance of the quantum state  $\rho$  to the nearest incoherent state  $\delta$  can be given as,

$$C_{tr}(\rho) = \min_{\delta \in \mathcal{I}} D(\rho, \delta) = \min_{\delta \in \mathcal{I}} \{\text{Tr}|\rho - \delta|\}, \quad (3.14)$$

where  $D(\rho, \delta) = \text{Tr}|\rho - \delta|$  is the trace-norm distance between  $\rho$  and  $\delta$ . A smaller  $C_{tr}(\rho)$  value implies that the state is closer to the nearest incoherent state, and hence, has less coherence. Conversely, a larger value indicates that the state is further away from the incoherent state, implying a higher degree of quantum coherence. It is still unknown whether  $C_{tr}$  obeys the strong monotonicity condition  $\mathbf{C}'_2$  in general.

However, for two-qubit Bell-diagonal states, such as those encountered in the two-flavor mode-entangled neutrino case, the trace norm of coherence  $C_{tr}$  coincides with the  $l_1$ -norm of coherence  $C_{l_1}$ , thereby making it a proper measure of coherence in this context<sup>6</sup>[52, 53]. As a result, for the two-flavor mixing scenario involving two-qubit neutrinos, the trace

---

<sup>6</sup>It is important to note that this equivalence between  $C_{tr}$  and  $C_{l_1}$  does not extend to general two-qubit states, where the relationship between these measures can differ significantly.

norm of coherence  $C_{tr}^{2f}(\rho_{\alpha,2})$  is effectively equal to the  $l_1$ -norm of coherence  $C_{l_1}^{2f}(\rho_{\alpha,2})$ , which can be computed using the expression provided in Eq. (3.5). For pure qubit states  $|\psi\rangle\langle\psi|$ , the nearest incoherent state is simply  $\delta = \rho_D = \text{diag}\{|\psi\rangle\langle\psi|\}$ , where  $\rho_D$  is the dephased state. However, this straightforward identification does not hold for states with dimensions higher than 2, i.e., for  $d > 2$ . For qutrits, determining the optimal incoherent state becomes more challenging unless specific one-qutrit density matrices are considered, for which the eigenvalues of  $\rho - \delta$  are calculable, thus enabling the computation of  $D(\rho, \delta)$ . When the incoherent Kraus operators  $K_\ell$  are restricted to  $2 \times 2$  and  $3 \times 3$  (or  $3 \times 2$ ) matrices, the measure satisfies the strong monotonicity condition  $\mathbf{C}'_2$  and thus qualifies as a proper measure of coherence.

It is well understood that obtaining an analytic expression for  $C_{tr}$  is challenging, even for relatively simple cases such as pure qutrits. This often necessitates the use of semidefinite programming methods that rely on symmetric extensions [71]. In [53], a thorough investigation into the strong monotonicity of  $C_{tr}$  across general quantum states was conducted, and no violations of the condition  $\mathbf{C}'_2$  were found. This led to the hypothesis that the strong monotonicity of  $C_{tr}$  might be universally satisfied by all quantum states <sup>7</sup> [51].

**Coherence concurrence:** A relatively new and rigorous measure of quantum coherence, known as coherence concurrence, was introduced in [55] to explore the interplay and interconversion between two fundamental aspects of quantumness: entanglement and coherence. This measure provides a deeper understanding of the relationship between these two critical quantum resources, especially in systems where both coherence and entanglement play significant roles. The coherence concurrence is particularly relevant in the study of complex quantum systems, where it serves as a valuable tool for analyzing and quantifying the intertwined nature of coherence and entanglement. The coherence concurrence is based on the  $\frac{d(d-1)}{2}$ -dimensional symmetric generalized GGM matrices, which serve as the symmetric generators of the  $SU(d)$  Lie-algebra. These matrices are instrumental in capturing the multi-level structure of quantum states in higher-dimensional systems. Specifically, the symmetric GGM matrices are given by  $\Lambda_s^{i,j} = |i\rangle\langle j| + |j\rangle\langle i|$ , where  $1 \leq i < j \leq d$ .

This measure satisfies all the stringent conditions required for a proper coherence measure:  $\mathbf{C}_1$ ,  $\mathbf{C}_2$ ,  $\mathbf{C}'_2$ , and  $\mathbf{C}_3$ . The coherence concurrence is defined as the convex-roof of the  $l_1$ -norm of coherence, which is expressed mathematically as:

$$C_c(\rho) = \min_{\{p_i, |\psi_i\rangle\}} \sum_i p_i C_{l_1}(|\psi_i\rangle\langle\psi_i|), \quad (3.15)$$

where the minimization is performed over all possible pure state decompositions of the mixed state  $\rho$ . Here,  $\rho$  is represented as  $\rho = \sum_i p_i |\psi_i\rangle\langle\psi_i|$ , where  $p_i$  denotes the probability of obtaining the  $i$ -th outcome, with  $p_i \geq 0$  and  $\sum_i p_i = 1$ . In the case of any dimensional pure state, such as the mode-entangled neutrino systems considered in this study, it has been shown that the coherence concurrence  $C_c(\rho)$  simplifies to the  $l_1$ -norm of coherence.

---

<sup>7</sup>The authors of [53] were unable to uniformly generate the incoherent channels.

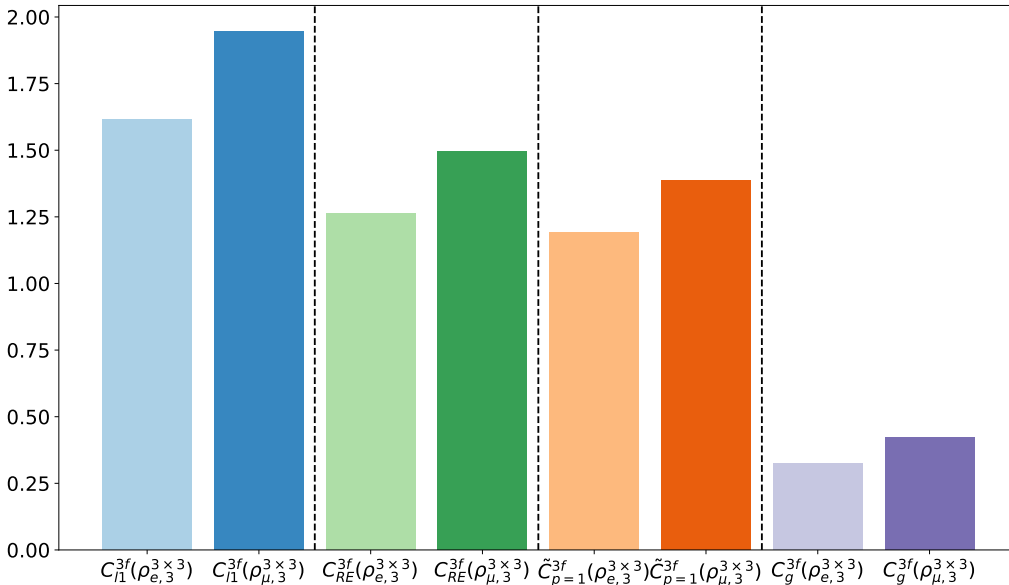


**Figure 2.** We depict the coherence measures  $C_{l_1}^{3f}(\rho_{\alpha,3}^{3\times 3})$ ,  $C_{RE}^{3f}(\rho_{\alpha,3}^{3\times 3})$ ,  $\tilde{C}_{p=1}^{3f}(\rho_{\alpha,3}^{3\times 3})$ , and  $C_g^{3f}(\rho_{\alpha,3}^{3\times 3})$  in blue, green, orange and purple shades respectively, for initial electron-neutrino states  $\alpha = e$  in the light-shaded bar and for initial muon-neutrino states  $\alpha = \mu$  in the dark-shaded bar. The bar plots are generated for three-flavor neutrino oscillations, where the neutrino state is represented as a three-mode system mapped onto the basis of a one-qutrit system.

### 3.2 Relative entropy of coherence

Among the various distance measures of coherence, the relative entropy of coherence—also known as *distillable coherence*—stands out as a fundamental canonical monotone. This measure holds particular significance as it can be operationally interpreted as the optimal rate at which one can distill a maximally coherent state from a given state  $\rho$  through incoherent CPTP operations  $\Xi_{\text{ICPTP}}(\rho)$  in the asymptotic limit of many copies of the state [50].

The quantum relative entropy, which quantifies the metric distance between two density matrices  $\rho$  and  $\sigma$ , is defined as:

$$S(\rho\|\sigma) = \text{Tr}[\rho(\log \rho - \log \sigma)] = -\text{Tr}[\rho(\log \sigma)] - S(\rho), \quad (3.16)$$

where  $\sigma \in \mathcal{I}$  represents an incoherent quantum state, and  $S(\rho) \equiv -\text{Tr}(\rho \log \rho)$  denotes the von Neumann entropy of  $\rho(t)$ . By applying Eq. (3.16), we obtain the difference in relative entropies as:

$$S(\rho_D\|\sigma) - S(\rho\|\sigma) = S(\rho) - S(\rho_D), \quad (3.17)$$

where  $\rho_D(t)$  is the dephased state, constructed by retaining only the diagonal elements of the density matrix  $\rho(t)$ . The *relative entropy of coherence* can thus be expressed in a closed-form as [48, 72],

$$C_{RE}(\rho) = S(\rho_D(t)) - S(\rho(t)) = \text{Tr}[\rho(t) \log \rho(t) - \rho_D(t) \log \rho_D(t)]. \quad (3.18)$$

In comparison to other measures, such as the  $l_1$ -norm, which captures coherence by summing the magnitudes of off-diagonal elements in the density matrix, the relative entropy of coherence offers a more profound and holistic understanding by encompassing the full informational content of the quantum state. Although the  $l_1$ -norm is advantageous for its simplicity and straightforward computation, it provides a more focused perspective, emphasizing only the contributions from off-diagonal components. On the other hand, the relative entropy of coherence assesses the overall distribution of coherence within the state and quantifies its potential as a quantum resource in practical applications. It gauges how distinguishable a quantum state is from its dephased, incoherent version, offering valuable insights into the state's effectiveness for quantum information processing tasks.

For our relevant pure states like  $|\nu_\alpha\rangle\langle\nu_\alpha|$  this measure is given as<sup>8</sup>,

$$C_{\text{RE}}(|\nu_\alpha\rangle\langle\nu_\alpha|) = S(\rho_{D\alpha}(t)) = -\text{Tr}[\rho_{D\alpha}(t) \log \rho_{D\alpha}(t)], \quad (3.19)$$

where  $\rho_{D\alpha}$  is the dephased state made out of the diagonal part of the pure density operator  $|\nu_\alpha\rangle\langle\nu_\alpha|$ . Using the density matrix in Eq. (2.6), we can write the relative entropy of coherence for the two-flavor oscillations of two-qubit neutrinos as,

$$\begin{aligned} C_{\text{RE}}^{2f}(\rho_{\alpha,2}^{4\times 4}) &= -\text{Tr}[\rho_{D\alpha,2}^{4\times 4}(\theta, L) \log \rho_{D\alpha,2}^{4\times 4}(\theta, L)] \\ &= -\left(|\tilde{U}_{\alpha\alpha}(\theta, L)|^2 \log(|\tilde{U}_{\alpha\alpha}(\theta, L)|^2) + |\tilde{U}_{\alpha\beta}(\theta, L)|^2 \log(|\tilde{U}_{\alpha\beta}(\theta, L)|^2)\right) \end{aligned} \quad (3.20)$$

where the survival probability  $|\tilde{U}_{\alpha\alpha}(\theta, L)|^2$  and the transition probability  $|\tilde{U}_{\alpha\beta}(\theta, L)|^2$  can be substituted using the coefficients from Eq. (2.5). We then get the  $C_{\text{RE}}^{2f}$  in terms of measurable parameters of oscillation as,

$$\begin{aligned} C_{\text{RE}}^{2f}(\rho_{\alpha,2}^{4\times 4}) &= -\left(\cos^4\theta + \sin^4\theta\right) \log\left(\cos^4\theta + \sin^4\theta + \frac{\sin^2 2\theta}{2} \cos\frac{\Delta m_{ji}^2 t}{2p}\right) \\ &\quad - \frac{\sin^2 2\theta}{2} \cos\frac{\Delta m_{ji}^2 t}{2p} \log\left\{\cos^4\theta + \sin^4\theta + \frac{\sin^2 2\theta}{2} \left(2\cos\frac{\Delta m_{ji}^2 t}{2p} - 1\right)\right\} \\ &\quad - \sin^2 2\theta \log\left(\sin 2\theta \sin\frac{\Delta m_{ji}^2 t}{4p}\right). \end{aligned} \quad (3.21)$$

Now we can take the density matrix  $\rho_{e,3}^{3\times 3}(\theta_{ij}, L)$  from Eq. (2.11) and calculate the relative entropy of coherence for the three-flavor oscillations of one-qutrit electron-neutrinos as follows:

$$\begin{aligned} C_{\text{RE}}^{3f}(\rho_{e,3}^{3\times 3}) &= -\text{Tr}[\rho_{De,3}^{3\times 3}(\theta_{ij}, L) \log \rho_{De,3}^{3\times 3}(\theta_{ij}, L)] \\ &= -2(c_{12}^2 c_{13}^2 \log(c_{12} c_{13}) + (s_{12} c_{13} + c_{12} s_{23} s_{13})^2 \log(s_{12} c_{13} - c_{12} s_{23} s_{13}) \\ &\quad + (s_{12} s_{23} - c_{12} c_{23} s_{13})^2 \log(s_{12} s_{23} - c_{12} c_{23} s_{13})), \end{aligned} \quad (3.22)$$

where the matrix elements  $\hat{\rho}_{e,ij}$  can be obtained from Eq. (2.14). Similarly, we can take the density matrix  $\rho_{\mu,3}^{3\times 3}(\theta_{ij}, L)$  from Eq. (2.12) and calculate the relative entropy of coherence

---

<sup>8</sup>Hereon, log represents binary logarithm, with base 2

for the three-flavor oscillations of one-qudit muon-neutrinos as,

$$\begin{aligned}
C_{\text{RE}}^{3f} \left( \rho_{\mu,3}^{3 \times 3} \right) &= -\text{Tr} \left[ \rho_{D\mu,3}^{3 \times 3}(\theta_{ij}, L) \log \rho_{D\mu,3}^{3 \times 3}(\theta_{ij}, L) \right] \\
&= -2 \left( s_{12}^2 c_{13}^2 \log(s_{12} c_{13}) + (c_{12} c_{13} - s_{12} s_{23} s_{13})^2 \log(c_{12} c_{13} - s_{12} s_{23} s_{13}) \right. \\
&\quad \left. + (c_{12} s_{23} + s_{12} c_{23} s_{13})^2 \log(c_{12} s_{23} + s_{12} c_{23} s_{13}) \right), \tag{3.23}
\end{aligned}$$

where the matrix elements  $\hat{\rho}_{\mu,ij}$  can be obtained from Eq. (2.15). Here, in the case of mapping the neutrino states to the one-qudit system, the relative entropy of coherence for three-flavor oscillations of the initial electron-neutrino state  $C_{\text{RE}}^{3f} \left( \rho_{e,3}^{3 \times 3} \right)$  saturates to 1.26 while the same in the case of the initial muon-neutrino state i.e.  $C_{\text{RE}}^{3f} \left( \rho_{\mu,3}^{3 \times 3} \right)$  saturates to 1.5. This has been shown in the top-right panel in Fig. 2.

For three-flavor mode oscillations, when the initial neutrino flavor states  $|\nu_\alpha\rangle$  are expressed in the tripartite three-qubit basis, we consider the three  $8 \times 8$  density matrices  $\rho_{\alpha,3}^{8 \times 8}(\theta_{ij}, L)$  from Eq. (2.9) and express the relative entropy of coherence as,

$$\begin{aligned}
C_{\text{RE}}^{3f} \left( \rho_{\alpha,3}^{8 \times 8} \right) &= -\text{Tr} \left[ \rho_{D\alpha,3}^{8 \times 8}(\theta_{ij}, L) \log \rho_{D\alpha,3}^{8 \times 8}(\theta_{ij}, L) \right] \\
&= -2 \sum_{\beta=e}^{\tau} |a_{\alpha\beta}(\theta_{ij}, L)|^2 \log |a_{\alpha\beta}(\theta_{ij}, L)| = - \sum_{\beta=e}^{\tau} P_{\alpha\beta}(\theta_{ij}, L) \log P_{\alpha\beta}(\theta_{ij}, L), \tag{3.24}
\end{aligned}$$

where the coefficients  $a_{\alpha\beta}(\theta_{ij}, L)$  for  $\alpha, \beta = \{e, \mu, \tau\}$  can be extracted from Eq. (2.8) and substituted into Eq. (3.24) to express it in terms of the oscillation parameters. For the initial flavor  $\alpha = e$ ,  $C_{\text{RE}}^{3f} \left( \rho_{e,3}^{8 \times 8} \right)$  can be expressed as,

$$\begin{aligned}
C_{\text{RE}}^{3f} \left( \rho_{e,3}^{8 \times 8} \right) &= -|a_{ee}(\theta_{ij}, L)|^2 \log |a_{ee}(\theta_{ij}, L)|^2 - |a_{e\mu}(\theta_{ij}, L)|^2 \log |a_{e\mu}(\theta_{ij}, L)|^2 \\
&\quad - |a_{e\tau}(\theta_{ij}, L)|^2 \log |a_{e\tau}(\theta_{ij}, L)|^2, \tag{3.25}
\end{aligned}$$

and for the initial flavor  $\alpha = \mu$ ,  $C_{\text{RE}}^{3f} \left( \rho_{\mu,3}^{8 \times 8} \right)$  can be expressed as,

$$\begin{aligned}
C_{\text{RE}}^{3f} \left( \rho_{\mu,3}^{8 \times 8} \right) &= -|a_{\mu\mu}(\theta_{ij}, L)|^2 \log |a_{\mu\mu}(\theta_{ij}, L)|^2 - |a_{e\mu}(\theta_{ij}, L)|^2 \log |a_{e\mu}(\theta_{ij}, L)|^2 \\
&\quad - |a_{\mu\tau}(\theta_{ij}, L)|^2 \log |a_{\mu\tau}(\theta_{ij}, L)|^2, \tag{3.26}
\end{aligned}$$

where, using Eq. (2.8), the probabilities as squared-modulus coefficients  $|a_{\alpha\beta}(\theta_{ij}, L)|^2$  for  $\beta = \{e, \mu, \tau\}$  appearing in the above Eqs. (3.25) and (3.26) can be given as,

$$|a_{\alpha\beta}(\theta_{ij}, L)|^2 = P_{\alpha\beta}(\theta_{ij}, L) = \delta_{\alpha\beta} - 4 \sum_{j>i=1}^3 \text{Re} \left( U_{\alpha j}^* U_{\beta j} U_{\alpha i} U_{\beta i}^* \right) \sin^2 \frac{\Delta m_{ji}^2}{4E} L, \tag{3.27}$$

where  $U_{\alpha i}$ ;  $\alpha = \{e, \mu, \tau\}$ ,  $i = \{1, 2, 3\}$  are the PMNS matrix elements as defined in Eq. (2.2). The explicit expressions for  $|a_{\alpha\beta}(\theta_{ij}, L)|^2$  matching the generic three-flavor probability expression in Eq. (3.27) has been calculated using the definitions in Eq. (2.8) and provided in Appendix A.2. The relationship between the relative entropy of coherence and the survival/oscillation probabilities for both initial muon-neutrino and electron-neutrino

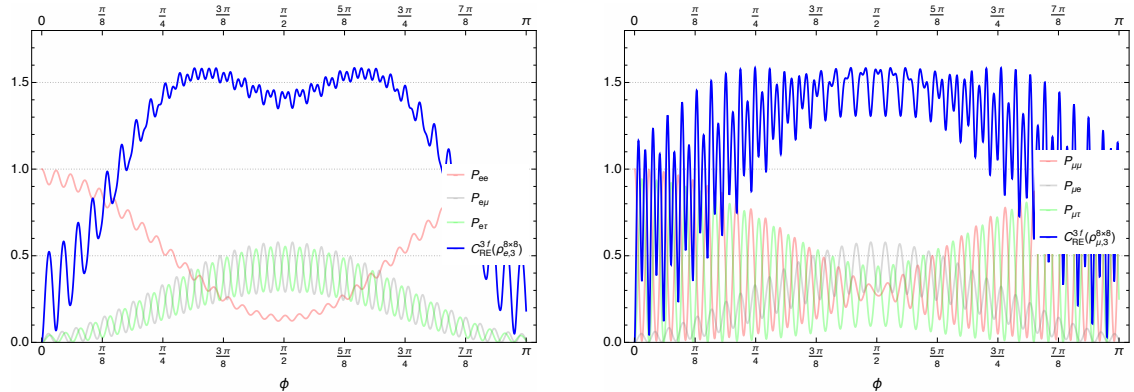


**Figure 3.** The figure displays the relative entropy of coherence  $C_{\text{RE}}^{3f}(\rho_{\mu,3}^{8 \times 8})$  (right panel) and  $C_{\text{RE}}^{3f}(\rho_{e,3}^{8 \times 8})$  (left panel), alongside the corresponding survival probability  $\nu_\mu \rightarrow \nu_\mu$  and transition probabilities  $\nu_\mu \rightarrow \nu_e$  and  $\nu_\mu \rightarrow \nu_\tau$  (right panel), as well as the probabilities  $\nu_e \rightarrow \nu_e$ ,  $\nu_e \rightarrow \nu_\mu$ , and  $\nu_e \rightarrow \nu_\tau$  (left panel). These quantities are plotted as functions of  $\phi$  which is defined as  $\phi = \frac{\Delta m_{21}^2 L}{4E}$ . The left-panel corresponds to the initial state of electron-neutrino and the right-panel corresponds to the initial state of muon-neutrino. This analysis pertains to three-flavor neutrino oscillations, with the neutrino state modelled as a three-mode system and mapped onto the tripartite basis of a three-qubit system.

states is illustrated in Fig. 3. The values of  $C_{\text{RE}}^{3f}(\rho_{\alpha,3}^{8 \times 8})$  correspond to the scenario where these neutrino states are mapped onto the tripartite basis of a three-qubit system. A high relative entropy of coherence indicates that the quantum state possesses a substantial amount of coherence, signifying that the state is far from being incoherent (classical) and maintains a significant degree of quantum superposition. This implies that the state can maintain and utilize quantum superpositions effectively.

The plots clearly demonstrate that, in both cases, the relative entropy of coherence inversely correlates with the survival probability of the initial neutrino flavor. This suggests that the value of coherence is high when the neutrino is less likely to stay in its original state, highlighting  $C_{\text{RE}}^{3f}(\rho_{\alpha,3}^{8 \times 8})$  as a robust indicator of oscillation activity. As the neutrino oscillates more frequently between different flavors, the coherence measure peaks, reflecting the system's heightened quantum behavior.

However, unlike the case of the  $l_1$ -norm of coherence, this inverse relationship is not exact, as the peak value of relative entropy of coherence does not correspond to the lowest value of the neutrino survival probability. Instead, it occurs at values of  $P_{\alpha\alpha}$  that are slightly higher than the minimum. For the initial  $\nu_e$  state, the peak value of  $C_{\text{RE}}^{3f}(\rho_{e,3}^{8 \times 8})$ , which is approximately 1.55, is attained at  $\phi \approx 5\pi/16$  and  $\phi \approx 13\pi/16$ , whereas the minimum of  $P_{ee}$  occurs at  $\phi = \pi/2$ . For the initial  $\nu_\mu$  state, the maximum of  $C_{\text{RE}}^{3f}(\rho_{\mu,3}^{8 \times 8})$ , which is approximately 1.6, is attained at  $\phi \approx \pi/4$  and  $\phi \approx 3\pi/4$ . Here again, the minimum of  $P_{\mu\mu}$  occurs at  $\phi = \pi/2$ . We can thus see that the maximum value of  $C_{\text{RE}}^{3f}(\rho_{\alpha,3}^{8 \times 8})$  exceeds the values of  $C_{\text{RE}}^{3f}(\rho_{\alpha,3}^{3 \times 3})$  as mentioned above (corresponding to the one-qutrit mapping) for both the initial flavor cases  $\alpha = e, \mu$ . This is due to the additional degrees of freedom that

the coupled higher dimensional three-qubit system enjoys over the single qutrit system. Additionally, it is clear that the relative entropy of coherence for the initial  $\nu_\mu$  state is slightly greater than that for the  $\nu_e$  state. This observation holds true for both the three-qubit and qutrit frameworks.

Furthermore, the plots reveal that coherence, as measured by  $C_{\text{RE}}^{3f}(\rho_{\alpha,3}^{8 \times 8})$ , remains significant throughout the entire cycle. Even when the survival probability is high,  $C_{\text{RE}}^{3f}(\rho_{\alpha,3}^{8 \times 8})$  does not drop to zero, indicating that the system retains some level of coherence even during periods of reduced oscillatory activity. Additionally, the multiple peaks observed in the relative entropy of coherence throughout the oscillation process suggest that the neutrino system experiences varying degrees of coherence as it propagates. These peaks align with the points where the oscillation probabilities between different flavors are also high, reinforcing the idea that coherence is intricately linked to the quantum mechanical nature of neutrino flavor oscillations.

**Coherence of formation** : The coherence of formation (or the *Intrinsic randomness measure*), which equals coherence cost, is the minimal asymptotic rate of consuming maximally coherent pure state for preparing  $\rho$  by incoherent operation [50]. Operationally, it represents the minimum amount of coherence required to generate a given quantum state using incoherent operations, making it a fundamental concept in the resource theory of coherence. For a pure state  $|\psi\rangle\langle\psi|$  (where  $|\psi\rangle = \sum_{i=1}^d a_i|i\rangle$ ) this measure is given as,

$$R_I(|\psi\rangle\langle\psi|) = S(\rho_D) = C_{\text{RE}}(|\psi\rangle\langle\psi|), \quad (3.28)$$

where  $\rho_D$  is the dephased state made out of the diagonal part of the pure state  $|\psi\rangle\langle\psi|$ , and  $C_{\text{RE}}$  is the relative entropy of coherence. Being the convex-roof of the relative entropy of coherence, Eq. (3.19) shows the equivalence of this measure with the relative entropy of coherence for pure states<sup>9</sup>. This measure can be physically interpreted as states with stronger coherence would, therefore, indicate larger randomness in measurement outcomes, and vice versa. Both the relative entropy of coherence and the coherence of formation are known to satisfy two additional conditions on top of the four conditions mentioned at the start of this section. One of these conditions is the condition of *uniqueness* for pure states is shown in Eqs. (3.19) and (3.28). The other condition is *additivity* under tensor products, i.e.,  $C(\rho \otimes \sigma) = C(\rho) + C(\sigma)$ , which are also satisfied by the logarithmic coherence rank.

### 3.3 Schatten- $p$ -norm-based functionals

The Schatten- $p$ -norm  $\|\cdot\|_p$  of any linear-bounded operator  $A$  is given by<sup>10</sup>,

$$\|A\|_p = \left( \text{Tr} \left[ \left( A^\dagger A \right)^{\frac{p}{2}} \right] \right)^{\frac{1}{p}}; \quad p \in [1, \infty), \quad (3.29)$$

<sup>9</sup>This coherence measure is extended to mixed state  $\rho$  by the convex roof construction (which inherently makes the measure satisfy the convexity property **C<sub>3</sub>**) as  $R_I(\rho) = \min_{\{p_i, |\psi_i\rangle\}} \sum_i p_i R_I(|\psi_i\rangle)$ , where the minimization is taken over all pure state decompositions and  $\rho = \sum_i p_i |\psi_i\rangle\langle\psi_i|$ .

<sup>10</sup>Here the case we are interested in is the  $p = 1$  trace class norm, other important values of  $p$  here include  $p = 2$  and  $p \rightarrow \infty$  corresponding to the Hilbert-Schmidt norm and the operator norm respectively.

The two classes of functionals used for measuring coherence, based on the aforementioned Schatten norm are given for  $p \geq 1$  as,

$$C_p = \min_{\delta \in \mathcal{I}} \|\rho - \delta\|_p, \quad \tilde{C}_p = \|\rho - \rho_D\|_p, \quad (3.30)$$

As per [54],

- $C_{p=1}$  is not a valid coherence measure under incoherent operations, strictly incoherent operations and genuinely incoherent operations<sup>11</sup>.
- $\tilde{C}_{p=1}$  is a valid coherence measure under both strictly incoherent operations and genuinely incoherent operations but NOT under incoherent operations.
- Neither  $C_{p>1}$  nor  $\tilde{C}_{p>1}$  is a valid coherence measure under any of the three sets of incoherent operations.

From the above points, it is reasonable to pursue the calculation of the second class of functionals based on the Schatten- $p = 1$ -norm given by,

$$\tilde{C}_{p=1}(\rho) = \text{Tr} \left[ \left( (\rho - \rho_D)^\dagger (\rho - \rho_D) \right)^{\frac{1}{2}} \right]. \quad (3.31)$$

The Schatten- $p = 1$ -norm-based functional offers a way to assess the coherence properties of neutrino states by measuring the extent to which the actual state differs from its dephased counterpart. This difference indicates the level of coherence, which is essential for understanding the entanglement and evolution of neutrino oscillations. Unlike other measures, such as the  $l_1$ -norm of coherence,  $\tilde{C}_{p=1}$  captures the overall distance between the density matrix and its dephased version, offering a more comprehensive perspective on coherence. While the  $l_1$ -norm primarily accounts for the sum of off-diagonal elements, the trace norm evaluates the entire matrix, making it a more encompassing measure in certain scenarios.

For the two-flavor mode entangled two-qubit neutrino system, we can take the density matrix in Eq. (2.6) and write this functional as,

$$\begin{aligned} \tilde{C}_{p=1}^{2f}(\rho_{\alpha,2}^{4 \times 4}) &= \text{Tr} \left[ \left\{ \left( \rho_{\alpha,2}^{4 \times 4}(\theta, L) - \rho_{D\alpha,2}^{4 \times 4}(\theta, L) \right)^\dagger \left( \rho_{\alpha,2}^{4 \times 4}(\theta, L) - \rho_{D\alpha,2}^{4 \times 4}(\theta, L) \right) \right\}^{\frac{1}{2}} \right] \\ &= 2|\tilde{U}_{\alpha\alpha}(\theta, L)| |\tilde{U}_{\alpha\beta}^*(\theta, L)|. \end{aligned} \quad (3.32)$$

Now substituting the coefficients from Eq. (2.5) in the above equation, we finally get,

$$\tilde{C}_{p=1}^{2f}(\rho_{\alpha,2}^{4 \times 4}) = 2 \sin 2\theta \sin \frac{\Delta m_{ji}^2 t}{4p} \sqrt{\left( \cos^4 \theta + \sin^4 \theta + \frac{\sin^2 2\theta}{2} \cos \frac{\Delta m_{ji}^2 t}{2p} \right)}, \quad (3.33)$$

---

<sup>11</sup>Genuinely incoherent operations are a subset of strictly incoherent operations, and the latter are a subset of incoherent operations.

where we have used  $E_i - E_j = \frac{\Delta m_{ij}^2}{2p}$  for  $i > j$ . Similarly, for the three-flavor mode entangled one-qudit neutrino system, we can take the density matrix  $\rho_{e(\mu),3}^{3 \times 3}(\theta_{ij}, L)$  from Eq. (2.11) (and Eq. (2.12)) and write this Schatten- $p = 1$ -norm based functional as,

$$\begin{aligned} \tilde{C}_{p=1}^{3f} \left( \rho_{e(\mu),3}^{3 \times 3} \right) &= \text{Tr} \left[ \left\{ \left( \rho_{e(\mu),3}^{3 \times 3}(\theta_{ij}, L) - \rho_{De(\mu),3}^{3 \times 3}(\theta_{ij}, L) \right)^\dagger \left( \rho_{e(\mu),3}^{3 \times 3}(\theta_{ij}, L) - \rho_{De(\mu),3}^{3 \times 3}(\theta_{ij}, L) \right) \right\}^{\frac{1}{2}} \right] \\ &= \sqrt{|\hat{\rho}_{e(\mu),12}|^2 + |\hat{\rho}_{e(\mu),13}|^2} + \sqrt{|\hat{\rho}_{e(\mu),12}|^2 + |\hat{\rho}_{e(\mu),23}|^2} + \sqrt{|\hat{\rho}_{e(\mu),13}|^2 + |\hat{\rho}_{e(\mu),23}|^2}, \end{aligned} \quad (3.34)$$

where the matrix elements  $\hat{\rho}_{e,ij}$  can be extracted from Eq. (2.14) to express  $\tilde{C}_{p=1}^{3f} \left( \rho_{e,3}^{3 \times 3} \right)$  in terms of measurable parameters as,

$$\begin{aligned} \tilde{C}_{p=1}^{3f} \left( \rho_{e,3}^{3 \times 3} \right) &= \sqrt{|-s_{12}^2 c_{23} s_{23} + s_{12} c_{12} c_{23}^2 s_{13} - c_{12} s_{23}^2 s_{13} s_{12} + c_{12}^2 s_{23} c_{23} s_{13}^2|^2} \\ &\quad + \sqrt{|s_{12} c_{23} c_{12} c_{13} + c_{12}^2 c_{13} s_{23} s_{13}|^2} \\ &\quad + \sqrt{|-s_{12}^2 c_{23} s_{23} + s_{12} c_{12} c_{23}^2 s_{13} - c_{12} s_{23}^2 s_{13} s_{12} + c_{12}^2 s_{23} c_{23} s_{13}^2|^2} \\ &\quad + \sqrt{|s_{12} s_{23} c_{12} c_{13} - c_{12}^2 c_{13} c_{23} s_{13}|^2} \\ &\quad + \sqrt{|s_{12} c_{23} c_{12} c_{13} + c_{12}^2 c_{13} s_{23} s_{13}|^2 + |s_{12} s_{23} c_{12} c_{13} - c_{12}^2 c_{13} c_{23} s_{13}|^2}, \end{aligned} \quad (3.35)$$

and the matrix elements  $\hat{\rho}_{\mu,ij}$  can be obtained from Eq. (2.15) to express  $\tilde{C}_{p=1}^{3f} \left( \rho_{\mu,3}^{3 \times 3} \right)$  in terms of measurable parameters as,

$$\begin{aligned} \tilde{C}_{p=1}^{3f} \left( \rho_{\mu,3}^{3 \times 3} \right) &= \sqrt{|-c_{12}^2 c_{23} s_{23} - s_{12} c_{12} c_{23}^2 s_{13} + c_{12} s_{23}^2 s_{13} s_{12} + s_{12}^2 s_{23} c_{23} s_{13}^2|^2} \\ &\quad + \sqrt{|s_{12} c_{12} c_{13} c_{23} - s_{12}^2 c_{13} s_{23} s_{13}|^2} \\ &\quad + \sqrt{|-c_{12}^2 c_{23} s_{23} - s_{12} c_{12} c_{23}^2 s_{13} + c_{12} s_{23}^2 s_{13} s_{12} + s_{12}^2 s_{23} c_{23} s_{13}^2|^2} \\ &\quad + \sqrt{|s_{12} s_{23} c_{12} c_{13} + s_{12}^2 c_{13} c_{23} s_{13}|^2} \\ &\quad + \sqrt{|s_{12} c_{12} c_{13} c_{23} - s_{12}^2 c_{13} s_{23} s_{13}|^2 + |s_{12} s_{23} c_{12} c_{13} + s_{12}^2 c_{13} c_{23} s_{13}|^2}, \end{aligned} \quad (3.36)$$

When the neutrino states are mapped to the basis of the one-qudit system, the Schatten- $p = 1$ -norm-based functional for three-flavor oscillations of the initial electron-neutrino state  $\tilde{C}_{p=1}^{3f} \left( \rho_{e,3}^{3 \times 3} \right)$  saturates to 1.19 while the same in the case of initial muon-neutrino state i.e.  $\tilde{C}_{p=1}^{3f} \left( \rho_{\mu,3}^{3 \times 3} \right)$  saturates to 1.38. These values have been shown in the bottom-left panel in Fig. 2 as bar plots.

Now, for the three-flavor mode entangled three-qubit neutrino system, we can take the

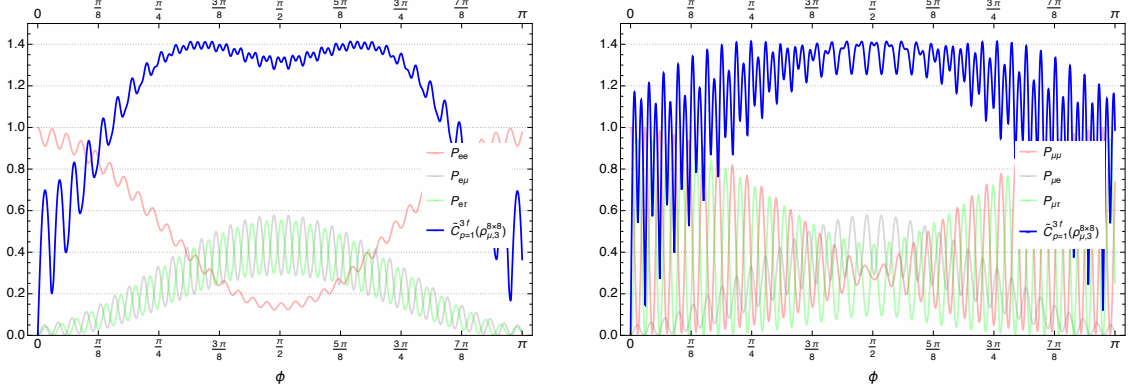


**Figure 4.** A plot of the Schatten- $p = 1$ -norm-based functional,  $\tilde{C}_{p=1}^{3f}(\rho_{\mu,3}^{8 \times 8})$  (right panel) and  $\tilde{C}_{p=1}^{3f}(\rho_{e,3}^{8 \times 8})$  (left panel), alongside the survival probability  $\nu_{\mu} \rightarrow \nu_{\mu}$  and the oscillation probabilities  $\nu_{\mu} \rightarrow \nu_e$  and  $\nu_{\mu} \rightarrow \nu_{\tau}$  (right panel) as well as the corresponding probabilities  $\nu_e \rightarrow \nu_e$ ,  $\nu_e \rightarrow \nu_{\mu}$ , and  $\nu_e \rightarrow \nu_{\tau}$  (left panel), for initial muon-neutrino (right-panel) and electron-neutrino states (left-panel), respectively, shown as a function of  $\phi$  which is defined as  $\phi = \frac{\Delta m_{21}^2}{4E}L$ . These plots correspond to three-flavor neutrino oscillations by mapping the neutrino state as a three-mode system to the tripartite basis of a three-qubit system.

density matrices from Eq. (2.9) and write this functional as,

$$\begin{aligned}
\tilde{C}_{p=1}^{3f}(\rho_{\alpha,3}^{8 \times 8}) &= \text{Tr} \left[ \left\{ \left( \rho_{\alpha,3}^{8 \times 8}(\theta_{ij}, L) - \rho_{D\alpha,3}^{8 \times 8}(\theta_{ij}, L) \right)^\dagger \left( \rho_{\alpha,3}^{8 \times 8}(\theta_{ij}, L) - \rho_{D\alpha,3}^{8 \times 8}(\theta_{ij}, L) \right) \right\}^{\frac{1}{2}} \right] \\
&= |a_{\alpha\tau}(\theta_{ij}, L)| \sqrt{|a_{\alpha\mu}(\theta_{ij}, L)|^2 + |a_{\alpha e}(\theta_{ij}, L)|^2} + |a_{\alpha\mu}(\theta_{ij}, L)| \sqrt{|a_{\alpha\tau}(\theta_{ij}, L)|^2 + |a_{\alpha e}(\theta_{ij}, L)|^2} \\
&+ |a_{\alpha e}(\theta_{ij}, L)| \sqrt{|a_{\alpha\mu}(\theta_{ij}, L)|^2 + |a_{\alpha\tau}(\theta_{ij}, L)|^2} \\
&= \sqrt{P_{\alpha\tau}(\theta_{ij}, L) (P_{\alpha\mu}(\theta_{ij}, L) + P_{\alpha e}(\theta_{ij}, L))} + \sqrt{P_{\alpha\mu}(\theta_{ij}, L) (P_{\alpha\tau}(\theta_{ij}, L) + P_{\alpha e}(\theta_{ij}, L))} \\
&+ \sqrt{P_{\alpha e}(\theta_{ij}, L) (P_{\alpha\mu}(\theta_{ij}, L) + P_{\alpha\tau}(\theta_{ij}, L))}, \tag{3.37}
\end{aligned}$$

where the coefficients  $a_{\alpha(e,\mu,\tau)}(\theta_{ij}, L)$  can be taken from Eq. (2.8) and substituted in the expression above.  $\tilde{C}_{p=1}^{3f}(\rho_{e,3}^{8 \times 8})$  can be expressed in terms of the three-flavor neutrino oscillation probabilities using the squared-modulus coefficients  $|a_{e\beta}(\theta_{ij}, L)|^2$ ;  $\beta = \{e, \mu, \tau\}$  in Eq. (3.27) for the initial flavor  $\alpha = e$ . Similarly,  $\tilde{C}_{p=1}^{3f}(\rho_{\mu,3}^{8 \times 8})$  can be expressed in terms of the oscillation probabilities  $|a_{\mu\beta}(\theta_{ij}, L)|^2$ ;  $\beta = \{e, \mu, \tau\}$  in Eq. (3.27) for the initial flavor  $\alpha = \mu$ .

Fig. 4 corresponds to the dynamics of the Schatten- $p = 1$ -norm-based functional  $\tilde{C}_{p=1}^{3f}(\rho_{\alpha,3}^{8 \times 8})$  for three-flavor neutrino oscillations, mapped to a tripartite basis of a one-qudit system. It can be seen from the plot that the Schatten- $p = 1$ -norm-based functional  $\tilde{C}_{p=1}^{3f}(\rho_{\alpha,3}^{8 \times 8})$  exhibits oscillatory behavior, similar to other coherence measures, reflecting the quantum coherence dynamics of the neutrino system. For both initial electron and muon neutrino states, the coherence measure oscillates between a minimum value near zero and a maximum value slightly above 1.4, which is again marginally greater than the

values of  $\tilde{C}_{p=1}^{3f}(\rho_{\alpha,3}^{3\times 3})$  for  $\alpha = e, \mu$  mentioned above, in the case of mapping of neutrino states to the basis of the one-qudit system. As with the  $l_1$ -norm and the relative entropy of coherence, the peaks in  $\tilde{C}_{p=1}^{3f}(\rho_{\alpha,3}^{3\times 3})$  tend to correspond to the intervals where the survival probability  $P_{\alpha\alpha}$  is low. This inverse relationship suggests that higher coherence, as quantified by the Schatten- $p = 1$ -norm, occurs when the neutrino is more likely to have oscillated into a different flavor, indicating rapid oscillation behavior. Notably,  $\tilde{C}_{p=1}^{3f}(\rho_{\alpha,3}^{3\times 3})$  does not drop to zero even at points where the oscillation probabilities suggest less frequent transitions. This indicates that the system maintains a baseline level of coherence throughout the entire oscillation cycle. Also, the peaks of this measure occur slightly before or after the complete disappearance of the initial flavor, indicating that the system retains some coherence even when it starts to transition back to the initial state.

The pattern of coherence dynamics is similar for both initial electron and muon neutrino states, though the specific locations of the peaks and troughs differ slightly due to the different mixing parameters involved in each case. For the electron neutrino case, the maximum coherence is observed around  $\phi = 5\pi/16$  and  $11\pi/16$ , while for the muon neutrino, similar behavior is observed for  $\phi = \pi/4$  and  $3\pi/4$ .

### 3.4 Geometric coherence as a fidelity-based measure

The geometric coherence is defined in general between two density operators  $\rho$  and  $\delta$  as,

$$C_g(\rho) = 1 - \max_{\delta \in \mathcal{I}} F(\rho, \delta), \quad (3.38)$$

where the fidelity is expressed as the square of the Uhlmann fidelity as  $F(\rho, \delta) = [\text{Tr}\sqrt{\rho^{1/2}\delta\rho^{1/2}}]^2$  is unity for  $\rho = \delta$ , and non-negative i.e., satisfying the condition **C**<sub>1</sub>. As the fidelity is non-decreasing under CPTP maps, it makes  $C_g(\rho)$  non-increasing under the action of  $\Xi_{\text{ICPTP}}$  and thus monotonic, satisfying **C**<sub>2</sub>. It also satisfies **C**'<sub>2</sub> and **C**<sub>3</sub> and is thus a proper measure.

Geometric coherence quantifies the distinguishability of a quantum state from the nearest incoherent state in a geometric sense, where “geometric” refers to the mathematical distance or proximity between states in the high-dimensional Hilbert space. This measure is based on fidelity, which evaluates the overlap between the quantum state  $\rho$  and the closest incoherent state  $\delta$ , providing a nuanced perspective on how far a state is from being incoherent. The geometric coherence captures this distance, making it particularly useful in assessing the robustness of coherence under various quantum transformations. This approach is valuable in practical scenarios like quantum computing and quantum metrology, where understanding how coherence is maintained or lost under operations is crucial. Unlike other coherence measures that focus on the total amount of coherence, geometric coherence offers an intuitive and geometrically grounded way to assess a quantum state’s coherence, particularly in terms of its resilience to noise and decoherence.

For pure states, the fidelity is given as  $F(\rho, \delta) = \text{Tr}(\rho\delta) = \sum_{i=1}^d \rho_{ii}\delta_i \leq \max_i \{\rho_{ii}\}$ , and thus the geometric coherence for pure states in  $d$ -dimensional Hilbert space becomes,

$$C_g(\rho) = 1 - \max_i \{\rho_{ii}\} = 1 - \frac{1}{d} - \frac{d-1}{d} \sqrt{1 - \frac{d}{d-1} \left(1 - \sum_i \rho_{ii}^2\right)}, \quad (3.39)$$

Now from the above Eq. (3.39), we can calculate the geometric coherence for two-flavor neutrino oscillations when neutrinos are mapped to two-qubit states ( $d = 4$ ) using the  $4 \times 4$  density matrix  $\rho_{\alpha,2}^{4 \times 4}(\theta, L)$  from Eq. (2.6) as,

$$\begin{aligned} C_g^{2f}(\rho_{\alpha,2}^{4 \times 4}) &= 1 - \max_i \{(\rho_{\alpha,2}^{4 \times 4})_{ii}\} = 1 - \max \{|\tilde{U}_{\alpha\alpha}(\theta, L)|^2, |\tilde{U}_{\alpha\beta}(\theta, L)|^2\} \\ &= \frac{3}{4} - \frac{3}{4} \sqrt{1 - \frac{4}{3} \left(1 - \left(|\tilde{U}_{\alpha\alpha}(\theta, L)|^4 + |\tilde{U}_{\alpha\beta}(\theta, L)|^4\right)\right)}, \end{aligned} \quad (3.40)$$

Putting the coefficients from Eq. (2.5) in the above equation Eq. (3.40), we get,

$$\begin{aligned} C_g^{2f}(\rho_{\alpha,2}^{4 \times 4}) &= 1 - \max \left\{ \cos^4 \theta + \sin^4 \theta + \frac{\sin^2 2\theta}{2} \cos \frac{\Delta m_{ij}^2}{2p}, \sin^2 2\theta \sin^2 \frac{\Delta m_{ij}^2}{4p} \right\} \\ &= \frac{1}{2} \left( \left| \cos^4 \theta + \sin^4 \theta + \frac{\sin^2 2\theta}{2} \left( \cos^2 \frac{\Delta m_{ij}^2}{4p} - 3 \sin^2 \frac{\Delta m_{ij}^2}{4p} \right) \right| \right. \\ &\quad \left. + \cos^4 \theta + \sin^4 \theta + \frac{\sin^2 2\theta}{2} \right). \end{aligned} \quad (3.41)$$

Now, for three-flavor mode-entangled oscillations of  $\nu_e$  mapped to one-qutrit states, we can express the geometric coherence through the density matrix  $\rho_{e,3}^{3 \times 3}(\theta_{ij}, L)$  from Eq. (2.11) as

$$C_g^{3f}(\rho_{e,3}^{3 \times 3}) = 1 - \max_i \{(\rho_{e,3}^{3 \times 3})_{ii}\} = 1 - \max \{c_{12}^2 c_{13}^2, (s_{12} c_{13} + c_{12} s_{23} s_{13})^2, (s_{12} s_{23} - c_{12} c_{23} s_{13})^2\}. \quad (3.42)$$

Similarly, for three-flavor oscillations of  $\nu_\mu$  as one-qutrit states, the geometric coherence through the density matrix  $\rho_{\mu,3}^{3 \times 3}(\theta_{ij}, L)$  from Eq. (2.12) becomes,

$$C_g^{3f}(\rho_{\mu,3}^{3 \times 3}) = 1 - \max_i \{(\rho_{\mu,3}^{3 \times 3})_{ii}\} = 1 - \max \{s_{12}^2 c_{13}^2, (c_{12} c_{13} - s_{12} s_{23} s_{13})^2, (c_{12} s_{23} + s_{12} c_{23} s_{13})^2\}. \quad (3.43)$$

Here, in the case of mapping of the neutrino states to the basis of the one-qutrit system, the geometric coherence for three-flavor oscillations of the initial electron-neutrino state  $C_g^{3f}(\rho_{e,3}^{3 \times 3})$  attains a value of 0.32 while the same in the case of the initial muon-neutrino state i.e.  $C_g^{3f}(\rho_{\mu,3}^{3 \times 3})$  attains the value 0.42. This has been depicted in the bottom-right panel in Fig. 2.

When the three-flavor neutrino states are mapped to the three-qubit system given by the density matrix  $\rho_{\alpha,3}^{8 \times 8}(\theta_{ij}, L)$  in Eq. (2.9), the geometric coherence takes the form,

$$\begin{aligned} C_g^{3f}(\rho_{\alpha,3}^{8 \times 8}) &= 1 - \max_i \{(\rho_{\alpha,3}^{8 \times 8})_{ii}\} = 1 - \max \{|a_{\alpha e}(\theta_{ij}, L)|^2, |a_{\alpha \mu}(\theta_{ij}, L)|^2, |a_{\alpha \tau}(\theta_{ij}, L)|^2\} \\ &= 1 - \max \{P_{\alpha e}(\theta_{ij}, L), P_{\alpha \mu}(\theta_{ij}, L), P_{\alpha \tau}(\theta_{ij}, L)\} \end{aligned} \quad (3.44)$$

where the coefficients  $a_{\alpha\beta}(\theta_{ij}, L)$  with  $\alpha, \beta = \{e, \mu, \tau\}$  can be taken from the relations in Eq. (2.8).  $C_g^{3f}(\rho_{e,3}^{8 \times 8}) = 1 - \max_i \{(\rho_{e,3}^{8 \times 8})_{ii}\}$  can be expressed in terms of the three-flavor oscillation probabilities using the squared-modulus coefficients  $|a_{e\beta}(\theta_{ij}, L)|^2$ ;  $\beta = \{e, \mu, \tau\}$

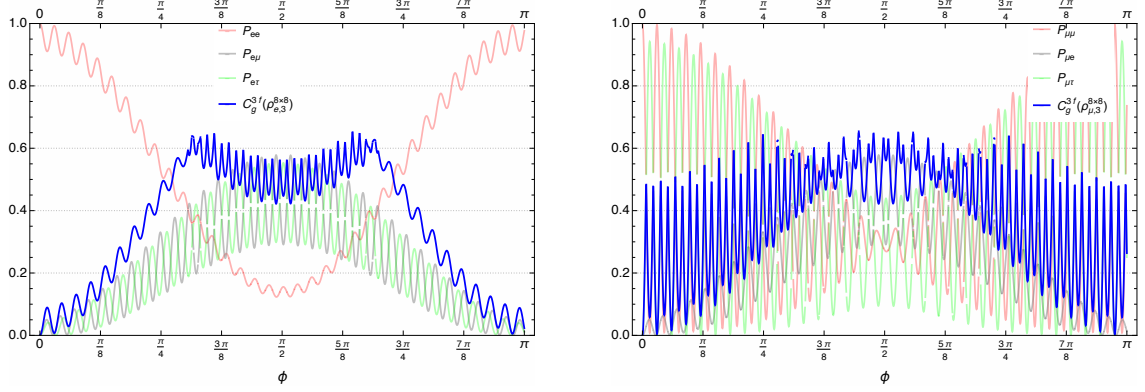


**Figure 5.** Displayed are the geometric coherence  $C_g^{3f}(\rho_{\mu,3}^{8\times 8})$  (right panel) and  $C_g^{3f}(\rho_{e,3}^{8\times 8})$  (left panel), along with the corresponding survival probability  $\nu_\mu \rightarrow \nu_\mu$  and transition probabilities  $\nu_\mu \rightarrow \nu_e$  and  $\nu_\mu \rightarrow \nu_\tau$  (right panel) and the probabilities  $\nu_e \rightarrow \nu_e$ ,  $\nu_e \rightarrow \nu_\mu$ , and  $\nu_e \rightarrow \nu_\tau$  (left panel). These results are plotted as a function of  $\phi$  which is defined as  $\phi = \frac{\Delta m_{21}^2}{4E} L$ . For initial muon-neutrino the plot has been given in the right-panel and for initial electron-neutrino in the left-panel. The analysis is performed for three-flavor neutrino oscillations, where the neutrino state is represented as a three-mode system mapped onto the tripartite basis of a three-qubit system.

shown in Eq. (3.27) for the initial flavor  $\alpha = e$ . Similarly,  $C_g^{3f}(\rho_{\mu,3}^{8\times 8}) = 1 - \max_i \{(\rho_{\mu,3}^{8\times 8})_{ii}\}$  can be expressed in terms of the oscillation probabilities  $|a_{\mu\beta}(\theta_{ij}, L)|^2$ ;  $\beta = \{e, \mu, \tau\}$  shown in Eq. (3.27) for the initial flavor  $\alpha = \mu$ .

The plots for geometric coherence  $C_g^{3f}(\rho_{\mu,3}^{8\times 8})$  and  $C_g^{3f}(\rho_{e,3}^{8\times 8})$ , Fig. 5, illustrate the coherence dynamics of neutrino oscillations for initial muon and electron neutrino states, respectively, mapped onto the tripartite basis of the three-qubit system. For the muon neutrino initial state, the plot of geometric coherence  $C_g^{3f}(\rho_{\mu,3}^{8\times 8})$  reveals a significant inverse correlation with the survival probability  $P_{\mu\mu}$  like other measures of coherence discussed in previous subsections. The coherence reaches its peak at points where the survival probability is at or near its lowest, indicating that the neutrino is most likely to transition to another flavor state at these moments. This behavior suggests that geometric coherence is strongly related to the flavor oscillation rate, with higher coherence corresponding to increased quantum superposition and oscillation activity between flavors.

Similarly, for the electron neutrino initial state, the plot of geometric coherence  $C_g^{3f}(\rho_{e,3}^{8\times 8})$  shows a comparable inverse relationship with the survival probability  $P_{ee}$ . The coherence peaks when the survival probability dips, again emphasizing the link between geometric coherence and the rate of flavor oscillation. The coherence remains non-zero throughout the entire cycle, indicating that even during periods of lower oscillatory activity, the system retains a notable degree of coherence. We see that  $C_g^{3f}(\rho_{\alpha,3}^{8\times 8})$  peaks around 0.65 for both the  $\nu_e$  and  $\nu_\mu$  initial states, which is more than both  $C_g^{3f}(\rho_{e,3}^{3\times 3})$  and  $C_g^{3f}(\rho_{\mu,3}^{3\times 3})$  which attain values around 0.325 and 0.424 respectively, as mentioned above for the case of mapping to the one-qutrit system. Thus again showcasing the additional degrees of freedom of the three-qubit system of neutrinos over the one-qutrit one. Both plots indicate that geometric coherence remains significant throughout the oscillation process, with multiple

peaks corresponding to the points of minimum survival probability. This sustained level of coherence reflects the underlying quantum mechanical nature of neutrino oscillations, where the system maintains coherence as it transitions between different flavors.

**Fidelity of coherence:** Another related measure called the fidelity of coherence is a measure based on the fidelity-induced distance between two states  $\rho$  and  $\delta$  and can be given as,

$$C_f(\rho) = 1 - \sqrt{\max_{\delta \in \mathcal{I}} F(\rho, \delta)}, \quad (3.45)$$

where again the non-decreasing property of fidelity  $F(\rho, \delta)$  under CPTP maps, makes the fidelity-induced distance  $1 - \sqrt{F(\rho, \delta)}$  and in turn  $C_f(\rho)$  monotonic. This measure satisfies the condition  $\mathbf{C}_2$ , but it has been shown in [51] using amplitude damping-like qubit ICPTP map,  $C_f(\rho)$  is a functional that does not qualify as a proper measure of coherence since it cannot be classified as “strong” monotone, i.e., it violates the strong monotonicity condition  $\mathbf{C}'_2$ <sup>12</sup>.

Although both geometric coherence and fidelity of coherence rely on fidelity, they approach the relationship between quantum states differently. Geometric coherence evaluates the highest fidelity across all incoherent states, whereas fidelity of coherence incorporates a square root function, potentially altering its sensitivity to specific quantum transformations.

### 3.5 Logarithmic coherence rank

The logarithmic coherence rank  $C_{\mathcal{L}}(|\psi\rangle)$  serves as a critical measure in the resource theory of coherence, offering unique insights into the structural complexity of quantum states. For pure states, the coherence number is the same as the coherence rank, and for mixed states, the coherence number is the smallest possible maximal coherence rank in any decomposition of the mixed state. For any pure state  $|\psi\rangle$  the logarithmic coherence rank is defined as [64],

$$C_{\mathcal{L}}(|\psi\rangle) = \log_2 R_C(|\psi\rangle) = \log_2 \left\{ \min_{|j\rangle \in \hat{\mathcal{O}}} \sum \lambda_j |j\rangle \right\}; \quad \hat{\mathcal{O}} \subseteq \mathcal{O}, \quad (3.46)$$

where  $\lambda_j$  are non-zero complex coefficients, and  $R_C(|\psi\rangle)$  is the coherence rank that represents the minimal number of the incoherent states in the fixed orthogonal basis  $\mathcal{O}$  in the decomposition of  $|\psi\rangle$ <sup>13</sup>. This measure characterizes the logarithm of the minimal number of incoherent states in the fixed orthogonal basis  $\mathcal{O}$  (in Hilbert space  $\mathcal{H}$ ) in such a decomposition of the pure state  $|\psi\rangle$ , thus revealing the multilevel nature of coherence. For a coherent pure state living in a  $d$ -dimensional Hilbert space, the minimum coherence rank is  $R_{C,min}(|\psi\rangle) = 2$ , while for the maximally coherent state,  $R_{C,max}(|\psi\rangle) = d$ . Hence, the logarithmic coherence rank satisfies the inequality  $1 \leq C_{\mathcal{L}}(|\psi\rangle) \leq \log_2 d$ .

As the coherence rank  $R_C(|\psi\rangle)$  provides a direct count of the minimal number of non-zero coefficients (incoherent states) required in the decomposition of a pure state,

<sup>12</sup>In general,  $C_f(\rho) \neq 1 - \sqrt{\text{Tr} \sqrt{\rho^{1/2} \rho_D \rho^{1/2}}}$  since the dephased state  $\rho_D$  is non necessarily optimal for the fidelity of coherence, making the subselection process hard to verify.

<sup>13</sup>For pure states in any  $d$ -dimensional Hilbert space, the coherence rank satisfies the inequality  $2 \leq R_C \leq d$

the logarithmic coherence rank then offers a more nuanced view by expressing this count in logarithmic terms, thereby reflecting the multilevel nature of coherence in terms of information content. This logarithmic scaling is particularly useful in comparing coherence across systems of different dimensions.

In comparison to other coherence measures like the  $l_1$ -norm or the relative entropy of coherence, the logarithmic coherence rank uniquely emphasizes the structural intricacies of the quantum state by counting the number of non-zero coefficients in its decomposition. While the  $l_1$ -norm and relative entropy are primarily concerned with quantifying the total coherence present in the state, the logarithmic coherence rank provides deeper insights into how coherence is distributed among the various components of the quantum state.

In practical terms, the logarithmic coherence rank's emphasis on the minimal number of significant components in a quantum state's decomposition can provide deeper insights into the operational capabilities of quantum systems, particularly in tasks like quantum computation, where the distribution of coherence directly impacts algorithmic efficiency. Further, in the context of quantum computing, a higher logarithmic coherence rank suggests an increased ability to encode and manipulate information, as a larger number of non-zero coefficients generally implies greater availability of quantum resources. Moreover, its logarithmic nature aligns well with the scaling of resources in quantum communication protocols, offering a valuable perspective in the study of high-dimensional quantum systems.

The definition of the measure in Eq. (3.46) can be extended to mixed states by the standard convex-roof construction, and we can thus define the logarithmic coherence number as [56],

$$C_{\mathcal{L}}(\rho) = \min_{\{p_i, |\psi_i\rangle\}} \sum_i p_i C_{\mathcal{L}}(|\psi_i\rangle), \quad (3.47)$$

where the minimization is taken over all pure state decompositions of  $\rho = \sum_i p_i |\psi_i\rangle\langle\psi_i|$ , wherein  $p_i$  is the probability of obtaining the  $i$ -th outcome. In [56],  $C_{\mathcal{L}}$  was established as a proper measure of coherence.

To begin with, in our two-qubit mode-entangled neutrino system, the decomposition of the two-flavor evolution, as given in Eq. (2.4), reveals that two out of the four possible coefficients are non-zero in the neutrino flavor state's decomposition in the Bell-basis. Notably, the coefficients corresponding to the Bell states  $|0\rangle \otimes |0\rangle$  and  $|1\rangle \otimes |1\rangle$  are zero, as evident from Eq. (2.4). Consequently, the coherence rank for this system is  $R_C(\rho_{\alpha,2}^{4 \times 4}) = 2$ , and the logarithmic coherence rank is  $C_{\mathcal{L}}^{2f}(\rho_{\alpha,2}^{4 \times 4}) = \log_2 2 = 1$ , which is depicted by the line-shaded section of the blue bar in Fig. 6.

In contrast, for the one-qutrit mode-entangled neutrino system, the decomposition of the three-flavor evolution (as per Eq. (2.10)) shows that all three coefficients are non-zero. Thus, the logarithmic coherence rank is  $C_{\mathcal{L}}^{3f}(\rho_{\alpha,3}^{3 \times 3}) = \log_2 3 = 1.585$ . This represents the maximum value of the logarithmic coherence rank for this system, signifying that the neutrino flavor state is maximally coherent in the one-qutrit basis, as illustrated by the fully line-shaded green bar in Fig. 6.

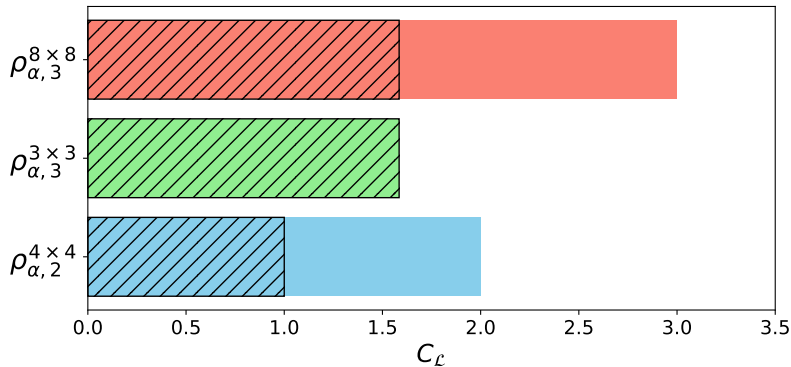


**Figure 6.** We show the maximum values of the logarithmic coherence rank  $C_{\mathcal{L},max}$  for the two-qubit system  $\rho_{\alpha,2}^{4 \times 4}$ , the one-qutrit system  $\rho_{\alpha,3}^{3 \times 3}$  and the three-qubit system  $\rho_{\alpha,3}^{8 \times 8}$  in blue, green and red respectively. We show the values of  $C_{\mathcal{L}}$  for our neutrino flavor states mapped to the aforementioned quantum systems as line-shaded bars.

Similarly, for the three-flavor evolution of the mode-entangled three-qubit neutrino system, there are three non-zero coefficients out of the possible eight in the decomposition within the tripartite basis of the three-qubit system (given in Eq. (2.7)). This yields the same logarithmic coherence rank  $\log_2 3$  as observed in the one-qutrit basis case. The logarithmic coherence rank  $C_{\mathcal{L}}^{3f}(\rho_{\alpha,3}^{8 \times 8})$  is represented by the line-shaded section of the red bar in Fig. 6.

This analysis highlights that the (logarithmic) coherence rank consistently equals the (logarithm of) the minimal number of non-zero coefficients in the multipartite basis of any dimensional entangled system. For a state with  $k$  non-zero coefficients  $\lambda_j$  in Eq. (3.46), the logarithmic coherence rank is  $C_{\mathcal{L}}(|\psi\rangle) = \log_2 k$ . For maximally coherent states  $|\psi_M\rangle$ , this becomes  $C_{\mathcal{L}}(|\psi_M\rangle) = \log_2 d$ , where  $d$  is the dimension of the Hilbert space.

Therefore, in the two-qubit system, the maximum logarithmic coherence rank is  $C_{\mathcal{L},max}(\rho_{\alpha,2}^{4 \times 4}) = \log_2 4 = 2$ ; in the one-qutrit system, it is  $C_{\mathcal{L},max}(\rho_{\alpha,3}^{3 \times 3}) = \log_2 3 = 1.585$ ; and in the three-qubit system, it is  $C_{\mathcal{L},max}(\rho_{\alpha,3}^{8 \times 8}) = \log_2 8 = 3$ . These values are represented in blue, green, and red, respectively, in Fig. 6.

## 4 Conclusions

In this comprehensive study, we have explored the profound interplay between quantum coherence and neutrino oscillations, framing neutrino flavor states within multi-mode quantum systems and analyzing them through the rigorous lens of quantum information theory. Recognizing quantum coherence as the cornerstone of all quantum correlations, our investigation has delved into its manifestation and evolution in neutrino systems. By providing a detailed methodology for calculating all relevant coherence measures in both two-flavor and three-flavor mixing scenarios, we have equipped the field with a methodological framework to facilitate future experimental and theoretical endeavors aimed at harnessing neutrinos for quantum technologies.

Our analysis extended beyond traditional measures of quantum coherence, such as the  $l_1$ -norm and relative entropy of coherence, to include a suite of sophisticated metrics like the Schatten- $p$ -norm-based functionals, geometric coherence and logarithmic coherence rank. Each measure provided unique insights:

- $l_1$ -norm of Coherence: This measure, applicable to general quantum states, serves as a baseline for evaluating coherence by quantifying the degree of superposition within neutrino states. For the neutrino state mapped onto the tripartite basis of the three-qubit system, the  $l_1$ -norm of coherence is closely linked to the neutrino oscillation rates. There is an inverse relationship between the  $l_1$ -norm and the survival probability, with the norm reaching its peak when the survival probability is at its lowest. This suggests that coherence is maximized during the periods of most active oscillation between neutrino flavors. In contrast, for the qutrit case, the  $l_1$ -norm of coherence remains fixed at a value slightly lower than the maximum observed in the three-qubit case, indicating a more stable coherence that does not vary with the oscillation dynamics. Furthermore, the  $l_1$ -norm remains non-zero throughout the entire oscillation process, signifying that the system retains quantum coherence even during periods of diminished oscillatory activity. The trace norm distance measure reduces to the  $l_1$ -norm of coherence for the two-flavor mode-entangled oscillations of neutrino states of the Bell-diagonal structure. Moreover, the measures of coherence such as the robustness of coherence and coherence concurrence, simplify to the  $l_1$ -norm of coherence for the neutrino states under consideration.
- Relative Entropy of Coherence: This measure offers a more refined understanding of quantum coherence by assessing the distance of the system from an incoherent (classical) state. Similar to the  $l_1$ -norm, the relative entropy of coherence exhibits an inverse relationship with the survival probability for the neutrino state mapped onto the tripartite basis of the three-qubit system. However, the peak coherence does not perfectly align with the minimum survival probability. Further, the relative entropy of coherence also remains non-zero throughout the oscillation process, indicating that the system retains quantum coherence even during phases of reduced oscillatory behavior. Additionally, for the qutrit case, the relative entropy of coherence remains constant at a value slightly lower than the maximum observed in the three-qubit framework. Moreover, the coherence of formation, also known as the intrinsic randomness measure, which equals the coherence cost, reduces to the relative entropy of coherence for the neutrino states under consideration.
- Schatten- $p$ -Norm-Based Functionals: These functionals are particularly sensitive to the nuances of entangled systems and provide deeper insights into quantum correlations beyond mere superposition. For the neutrino state mapped onto the tripartite basis of the three-qubit system, it exhibits a pronounced inverse relationship with survival probability, reaching its peak when the survival probability is near to its lowest value, highlighting its sensitivity to the subtleties of entangled states and oscillation dynamics. Additionally, these functionals remain consistently non-zero throughout

the oscillation cycle, indicating the robustness of coherence in the system, even as the intensity of oscillations fluctuates. Further, for the qutrit case, this metric remains constant at a value slightly below the maximum observed in the three-qubit framework.

- **Geometric Coherence:** By interpreting coherence as the minimal distance to the set of incoherent states, this measure provided a geometric perspective on the quantumness of neutrino oscillations. Like other measures of coherence, geometric coherence also displays a clear inverse correlation with survival probability for the case when the neutrino state is mapped onto the tripartite basis of the three-qubit system. Further, geometric coherence also maintains a non-zero value across the entire cycle, reflecting the continuous presence of coherence even during phases of diminished oscillatory behavior. Moreover, in the qutrit framework, this measure remains constant at a value slightly lower than the peak observed in the three-qubit system.
- **Logarithmic Coherence Rank:** This measure captures the structural complexity of the quantum state in terms of the number of non-zero coefficients in its decomposition. Particularly, it increases logarithmically with the lower value for the two-qubit neutrino system and the higher value for the one-qutrit and three-qubit system since the minimum number of non-zero coefficients (quantified by the coherence rank) in the decomposition of the flavor state in the basis of the one-qutrit and three-qubit system is three and the same in the basis of the two-qubit system is two. Hence, this measure offers a nuanced view of coherence that reflects the multilevel nature of quantum systems, making it particularly insightful in comparing coherence across systems of different dimensions.

Thus we observe that apart from having an inverse relationship between the neutrino survival probability and the measures of coherence such as the  $l_1$ -norm, relative entropy of coherence, Schatten- $p$ -norm-based functionals and geometric coherence, we find that these measures remain non-zero throughout the entire oscillation cycle, even when the rate of oscillation is minimal. This resilience of coherence is evident for both initial electron-neutrino and muon-neutrino states, highlighting the persistent quantum nature of the system. Furthermore, a notable common feature across these measures is that the coherence values are marginally higher for the initial muon-neutrino state compared to the electron-neutrino state, suggesting a subtle but consistent difference in the coherence dynamics between these two cases. This is true for both frameworks, i.e., when the neutrinos are mapped to a three-qubit system and when they are mapped to a qutrit.

Additionally, we find that measures like the relative entropy of coherence, Schatten- $p$ -norm-based functionals, and geometric coherence can be expressed in terms of neutrino oscillation probabilities, which are directly measurable in experiments. This implies that these quantifiers of quantum coherence can be experimentally observed in various neutrino oscillation setups.

In conclusion, this work not only advances our understanding of the quantum mechanical fabric of neutrino oscillations but also lays the groundwork for leveraging these

fundamental particles in the burgeoning arena of quantum information science. By applying a range of coherence measures, we have deepened our understanding of the quantum mechanical behavior of neutrinos, highlighting their potential as resources for quantum information tasks. The symbiosis of neutrino physics and quantum information theory, as explored in this study, heralds a promising frontier for both foundational understanding as well as highlighting the potential of neutrinos for quantum technologies.

## 5 Acknowledgements

This work is dedicated to our friend and colleague Prof. Ashutosh K. Alok, who passed away during the final stages of manuscript preparation. NRSC would like to express sincere thanks to the Galileo Galilei Institute for Theoretical Physics, Florence, for their generous hospitality while completing part of this work. NRSC also wishes to express deep gratitude to the Department of Physics ‘‘E.R. Caianiello’’ and INFN, Salerno, for their generous hospitality and support during the early stages of this project.

## A Products of the coefficients $a_{\alpha\beta}(\theta_{ij}, L)$

### A.1 Evaluation of $|a_{\alpha\beta}^*(\theta_{ij}, L) a_{\alpha\gamma}(\theta_{ij}, L)|$ , $\beta \neq \gamma$

The products  $|a_{e\beta}^*(\theta_{ij}, L) a_{e\gamma}(\theta_{ij}, L)|$  appearing in the expression of  $C_{l_1}^{3f}(\rho_{e,3}^{8\times 8})$  are given as,

$$\begin{aligned}
|a_{ee}^*(\theta_{ij}, L) a_{e\mu}(\theta_{ij}, L)| &= \left| - (c_{12}^3 c_{13}^3 s_{12} c_{23} + c_{12}^4 c_{13}^3 s_{23} s_{13}) + (s_{12}^3 c_{13}^3 c_{12} c_{23} - s_{12}^4 c_{13}^3 s_{23} s_{13}) \right. \\
&\quad \left. + s_{13}^3 s_{23} c_{13} + \{ (s_{12} c_{13}^3 c_{12}^2 c_{23} - s_{12}^2 c_{13}^3 s_{23} s_{13} c_{12}^2) \right. \\
&\quad \left. - (c_{12} c_{13}^3 s_{12}^3 c_{23} + c_{12}^2 c_{13}^3 s_{23} s_{13} s_{12}^2) \} \cos \frac{\Delta m_{21}^2}{2E} L + \{ s_{13} s_{23} c_{12}^2 c_{13}^3 \right. \\
&\quad \left. - (c_{12} c_{13} s_{12} c_{23} s_{13}^2 + c_{12}^2 c_{13} s_{23} s_{13}^3) \} \cos \frac{\Delta m_{31}^2}{2E} L + \{ s_{13} s_{23} c_{13}^3 s_{12}^2 \right. \\
&\quad \left. + (s_{12} c_{13} c_{12} c_{23} s_{13}^2 - s_{12}^2 c_{13} s_{23} s_{13}^3) \} \cos \frac{\Delta m_{32}^2}{2E} L \right|,
\end{aligned}$$

$$\begin{aligned}
|a_{ee}^*(\theta_{ij}, L) a_{e\tau}(\theta_{ij}, L)| &= \left| (c_{12}^3 c_{13}^3 s_{12} s_{23} - c_{12}^4 c_{13}^3 c_{23} s_{13}) - (s_{12}^3 c_{13}^3 c_{12} s_{23} + s_{12}^4 c_{13}^3 c_{23} s_{13}) \right. \\
&\quad \left. + s_{13}^3 c_{23} c_{13} + \{ (c_{12} c_{13}^3 s_{12}^3 s_{23} - c_{12}^2 c_{13}^3 c_{23} s_{13} s_{12}^2) \right. \\
&\quad \left. - (s_{12} c_{13}^3 c_{12}^2 s_{23} + s_{12}^2 c_{13}^3 c_{23} s_{13} c_{12}^2) \} \cos \frac{\Delta m_{21}^2}{2E} L + \{ s_{13} c_{23} c_{13}^3 c_{12}^2 \right. \\
&\quad \left. + (c_{12} c_{13} s_{12} s_{23} s_{13}^2 - c_{12}^2 c_{13} c_{23} s_{13}^3) \} \cos \frac{\Delta m_{31}^2}{2E} L + \{ s_{13} c_{23} c_{13}^3 s_{12}^2 \right. \\
&\quad \left. - (s_{12} c_{13} c_{12} s_{23} s_{13}^2 + s_{12}^2 c_{13} c_{23} s_{13}^3) \} \cos \frac{\Delta m_{32}^2}{2E} L \right|,
\end{aligned}$$

$$\begin{aligned}
|a_{e\mu}^*(\theta_{ij}, L) a_{e\tau}(\theta_{ij}, L)| = & \left| - (c_{12}c_{13}s_{12}c_{23} + c_{12}^2c_{13}s_{23}s_{13})(c_{12}c_{13}s_{12}s_{23} - c_{12}^2c_{13}c_{23}s_{13}) \right. \\
& - (s_{12}c_{13}c_{12}c_{23} - s_{12}^2c_{13}s_{23}s_{13})(s_{12}c_{13}c_{12}s_{23} + s_{12}^2c_{13}c_{23}s_{13}) \\
& + s_{13}c_{23}s_{23}c_{13} + \{ (c_{12}c_{13}s_{12}c_{23} + c_{12}^2c_{13}s_{23}s_{13})(s_{12}c_{13}c_{12}s_{23} \\
& + s_{12}^2c_{13}c_{23}s_{13}) + (s_{12}c_{13}c_{12}c_{23} - s_{12}^2c_{13}s_{23}s_{13})(c_{12}c_{13}s_{12}s_{23} \\
& - c_{12}^2c_{13}c_{23}s_{13}) \} \cos \frac{\Delta m_{21}^2}{2E} L + \{ (c_{12}c_{13}^2s_{12}s_{23}^2s_{13} \\
& - c_{12}^2c_{13}^2c_{23}s_{13}^2s_{23}) - (c_{12}c_{13}^2s_{12}c_{23}^2s_{13} + c_{12}^2c_{13}^2s_{23}s_{13}^2c_{23}) \} \cos \frac{\Delta m_{31}^2}{2E} L \\
& + \{ (s_{12}c_{13}^2c_{12}c_{23}^2s_{13} - s_{12}^2c_{13}^2s_{23}s_{13}^2c_{23}) - (s_{12}c_{13}^2c_{12}s_{23}^2s_{13} \\
& + s_{12}^2c_{13}^2c_{23}s_{13}^2s_{23}) \} \cos \frac{\Delta m_{32}^2}{2E} L \Big|. \tag{A.1}
\end{aligned}$$

The products  $|a_{\mu\beta}^*(\theta_{ij}, L) a_{\mu\gamma}(\theta_{ij}, L)|$  appearing in the expression of  $C_{l_1}^{3f}(\rho_{\mu,3}^{8 \times 8})$  are given as,

$$\begin{aligned}
|a_{e\mu}^*(\theta_{ij}, L) a_{\mu\mu}(\theta_{ij}, L)| = & \left| - (c_{12}c_{13}s_{12}c_{23} + c_{12}^2c_{13}s_{23}s_{13})(s_{12}c_{23} + c_{12}s_{23}s_{13})^2 + (s_{13}s_{23}^3c_{13}^3) \right. \\
& + (s_{12}c_{13}c_{12}c_{23} - s_{12}^2c_{13}s_{23}s_{13})(c_{12}c_{23} - s_{12}s_{23}s_{13})^2 + \{ - (c_{12}c_{13}s_{12}c_{23} \\
& + c_{12}^2c_{13}s_{23}s_{13})(c_{12}c_{23} - s_{12}s_{23}s_{13})^2 + (s_{12}c_{13}c_{12}c_{23} - s_{12}^2c_{13}s_{23}s_{13}) \\
& (s_{12}c_{23} + c_{12}s_{23}s_{13})^2 \} \cos \frac{\Delta m_{21}^2}{2E} L + \{ - (c_{12}c_{13}^3s_{12}c_{23}s_{23}^2 \\
& + c_{12}^2c_{13}^3s_{23}^3s_{13}) + (s_{13}s_{23}c_{13})(s_{12}c_{23} + c_{12}s_{23}s_{13})^2 \} \cos \frac{\Delta m_{31}^2}{2E} L \\
& + \{ (s_{12}c_{13}^3c_{12}c_{23}s_{23}^2 - s_{12}^2c_{13}^3s_{23}^3s_{13}) + (s_{13}s_{23}c_{13})(c_{12}c_{23} \\
& - s_{12}s_{23}s_{13})^2 \} \cos \frac{\Delta m_{32}^2}{2E} L \Big|,
\end{aligned}$$

$$\begin{aligned}
|a_{e\mu}^*(\theta_{ij}, L) a_{\mu\tau}(\theta_{ij}, L)| = & \left| - (c_{12}c_{13}s_{12}c_{23} + c_{12}^2c_{13}s_{23}s_{13})(-s_{12}^2c_{23}s_{23} + s_{12}c_{23}^2c_{12}s_{13} - c_{12}s_{23}^2s_{13}s_{12} \right. \\
& + c_{12}^2s_{23}s_{13}^2c_{23}) + (s_{12}c_{13}c_{12}c_{23} - s_{12}^2c_{13}s_{23}s_{13})(-c_{12}^2c_{23}s_{23} - c_{12}c_{23}^2s_{12}s_{13} \\
& + s_{12}s_{23}^2s_{13}c_{12} + s_{12}^2c_{23}s_{13}^2s_{23}) + \{ (c_{12}c_{13}s_{12}c_{23} + c_{12}^2c_{13}s_{23}s_{13})(-c_{12}^2c_{23}s_{23} \\
& - c_{12}c_{23}^2s_{12}s_{13} + s_{12}s_{23}^2s_{13}c_{12} + s_{12}^2c_{23}s_{13}^2s_{23}) - (s_{12}c_{13}c_{12}c_{23} \\
& - s_{12}^2c_{13}s_{23}s_{13})(-s_{12}^2c_{23}s_{23} + s_{12}c_{23}^2c_{12}s_{13} - c_{12}s_{23}^2s_{13}s_{12} \\
& + c_{12}^2s_{23}s_{13}^2c_{23}) \} \cos \frac{\Delta m_{21}^2}{2E} L + s_{13}s_{23}^2c_{13}^3c_{23} + \{ (-s_{12}^2c_{23}s_{23}^2s_{13}c_{13} \\
& + s_{12}c_{23}^2c_{12}s_{13}^2s_{23}c_{13} - c_{12}s_{23}^3s_{13}^2s_{12}c_{13} + c_{12}^2s_{23}^2s_{13}^3c_{23}c_{13}) - (c_{12}c_{13}^3s_{12}c_{23}^2s_{23} \\
& + c_{12}^2c_{13}^3s_{23}^2s_{13}c_{23}) \} \cos \frac{\Delta m_{31}^2}{2E} L + \{ (s_{12}c_{13}^3c_{12}c_{23}^2s_{23} - s_{12}^2c_{13}^3s_{23}^2s_{13}c_{23}) \\
& + (-c_{12}^2c_{23}s_{23}^2s_{13}c_{13} - c_{12}c_{23}^2s_{12}s_{13}^2s_{23}c_{13} + s_{12}s_{23}^3s_{13}^2c_{12}c_{13} \\
& + s_{12}^2c_{23}s_{13}^3s_{23}^2c_{13}) \} \cos \frac{\Delta m_{32}^2}{2E} L \Big|,
\end{aligned}$$

$$\begin{aligned}
|a_{\mu\mu}^*(\theta_{ij}, L) a_{\mu\tau}(\theta_{ij}, L)| = & \left| (-s_{12}^2 c_{23} s_{23} + s_{12} c_{23}^2 c_{12} s_{13} - c_{12} s_{23}^2 s_{13} s_{12} + c_{12}^2 s_{23} s_{13}^2 c_{23})(s_{12} c_{23} \right. \\
& + c_{12} s_{23} s_{13})^2 + (-c_{12}^2 c_{23} s_{23} - c_{12} c_{23}^2 s_{12} s_{13} + s_{12} s_{23}^2 s_{13} c_{12} + s_{12}^2 c_{23} s_{13}^2 s_{23}) \\
& (c_{12} c_{23} - s_{12} s_{23} s_{13})^2 + s_{23}^3 c_{13}^4 c_{23} + \{(-c_{12}^2 c_{23} s_{23} - c_{12} c_{23}^2 s_{12} s_{13} \\
& + s_{12} s_{23}^2 s_{13} c_{12} + s_{12}^2 c_{23} s_{13}^2 s_{23})(s_{12} c_{23} + c_{12} s_{23} s_{13})^2 + (-s_{12}^2 c_{23} s_{23} \\
& + s_{12} c_{23}^2 c_{12} s_{13} - c_{12} s_{23}^2 s_{13} s_{12} + c_{12}^2 s_{23} s_{13}^2 c_{23})(c_{12} c_{23} \\
& - s_{12} s_{23} s_{13})^2 \} \cos \frac{\Delta m_{21}^2}{2E} L + \{(-s_{12}^2 c_{23} s_{23}^3 c_{13}^2 + s_{12} c_{23}^2 c_{12} s_{13} s_{23}^2 c_{13}^2 \\
& - c_{12} s_{23}^4 s_{13} s_{12} c_{13}^2 + c_{12}^2 s_{23}^3 s_{13}^2 c_{23} c_{13}^2) + (s_{23} c_{13}^2 c_{23})(s_{12} c_{23} \\
& + c_{12} s_{23} s_{13})^2 \} \cos \frac{\Delta m_{31}^2}{2E} L + \{(s_{23} c_{13}^2 c_{23})(c_{12} c_{23} - s_{12} s_{23} s_{13})^2 \\
& + (-c_{12}^2 c_{23} s_{23}^3 c_{13}^2 - c_{12} c_{23}^2 s_{12} s_{13} s_{23}^2 c_{13}^2 + s_{12} s_{23}^4 s_{13} c_{12} c_{13}^2 \\
& + s_{12}^2 c_{23} s_{13}^2 s_{23}^3 c_{13}^2) \} \cos \frac{\Delta m_{32}^2}{2E} L. \tag{A.2}
\end{aligned}$$

## A.2 Evaluation of the probabilities $|a_{\alpha\beta}(\theta_{ij}, L)|^2$

The three-flavor oscillation probabilities  $P_{\alpha\beta} = |a_{\alpha\beta}(\theta_{ij}, L)|^2$  appearing in the expression of  $C_{\text{RE}}^{3f}(\rho_{\alpha,3}^{8 \times 8})$ ,  $\tilde{C}_{p=1}^{3f}(\rho_{\alpha,3}^{8 \times 8})$  and  $C_g^{3f}(\rho_{\alpha,3}^{8 \times 8})$  are given as,

$$\begin{aligned}
|a_{ee}(\theta_{ij}, L)|^2 = & c_{12}^4 c_{13}^4 + s_{12}^4 c_{13}^4 + s_{13}^4 + s_{12}^2 c_{13}^4 c_{12}^2 \cos \frac{\Delta m_{21}^2}{2E} L + c_{12}^2 c_{13}^2 s_{13}^2 \cos \frac{\Delta m_{31}^2}{2E} L \\
& + s_{12}^2 c_{13}^2 s_{13}^2 \cos \frac{\Delta m_{32}^2}{2E} L,
\end{aligned}$$

$$\begin{aligned}
|a_{\mu\mu}(\theta_{ij}, L)|^2 = & (s_{12} c_{23} + c_{12} s_{23} s_{13})^4 + (c_{12} c_{23} - s_{12} s_{23} s_{13})^4 + s_{23}^4 c_{13}^4 \\
& + (s_{12} c_{23} + c_{12} s_{23} s_{13})^2 (c_{12} c_{23} - s_{12} s_{23} s_{13})^2 \cos \frac{\Delta m_{21}^2}{2E} L + s_{23}^2 c_{13}^2 (s_{12} c_{23} \\
& + c_{12} s_{23} s_{13})^2 \cos \frac{\Delta m_{31}^2}{2E} L + s_{23}^2 c_{13}^2 (c_{12} c_{23} - s_{12} s_{23} s_{13})^2 \cos \frac{\Delta m_{32}^2}{2E} L,
\end{aligned}$$

$$\begin{aligned}
|a_{e\mu}(\theta_{ij}, L)|^2 = & (c_{12} c_{13} s_{12} c_{23} + c_{12}^2 c_{13} s_{23} s_{13})^2 + (s_{12} c_{13} c_{12} c_{23} - s_{12}^2 c_{13} s_{23} s_{13})^2 + s_{13}^2 s_{23}^2 c_{13}^2 \\
& - (c_{12} c_{13} s_{12} c_{23} + c_{12}^2 c_{13} s_{23} s_{13})(s_{12} c_{13} c_{12} c_{23} - s_{12}^2 c_{13} s_{23} s_{13}) \cos \frac{\Delta m_{21}^2}{2E} L \\
& - (c_{12} c_{13}^2 s_{12} c_{23} s_{13} s_{23} + c_{12}^2 c_{13}^2 s_{23}^2 s_{13}^2) \cos \frac{\Delta m_{31}^2}{2E} L + (s_{12} c_{13}^2 c_{12} c_{23} s_{13} s_{23} \\
& - s_{12}^2 c_{13}^2 s_{23}^2 s_{13}^2) \cos \frac{\Delta m_{32}^2}{2E} L,
\end{aligned}$$

$$\begin{aligned}
|a_{e\tau}(\theta_{ij}, L)|^2 = & (c_{12} c_{13} s_{12} s_{23} - c_{12}^2 c_{13} c_{23} s_{13})^2 + (s_{12} c_{13} c_{12} s_{23} + s_{12}^2 c_{13} c_{23} s_{13})^2 + s_{13}^2 c_{23}^2 c_{13}^2 \\
& - (c_{12} c_{13} s_{12} s_{23} - c_{12}^2 c_{13} c_{23} s_{13})(s_{12} c_{13} c_{12} s_{23} + s_{12}^2 c_{13} c_{23} s_{13}) \cos \frac{\Delta m_{21}^2}{2E} L \\
& + (c_{12} c_{13}^2 s_{12} s_{23} s_{13} c_{23} - c_{12}^2 c_{13}^2 c_{23}^2 s_{13}^2) \cos \frac{\Delta m_{31}^2}{2E} L - (s_{12} c_{13}^2 c_{12} s_{23} s_{13} c_{23} \\
& + s_{12}^2 c_{13}^2 c_{23}^2 s_{13}^2) \cos \frac{\Delta m_{32}^2}{2E} L,
\end{aligned}$$

$$\begin{aligned}
|a_{\mu\tau}(\theta_{ij}, L)|^2 = & (-s_{12}^2 c_{23} s_{23} + s_{12} c_{23}^2 c_{12} s_{13} - c_{12} s_{23}^2 s_{13} s_{12} + c_{12}^2 s_{23} s_{13}^2 c_{23})^2 + (-c_{12}^2 c_{23} s_{23} \\
& - c_{12} c_{23}^2 s_{12} s_{13} + s_{12} s_{23}^2 s_{13} c_{12} + s_{12}^2 c_{23} s_{13}^2 s_{23})^2 + (-s_{12}^2 c_{23} s_{23} + s_{12} c_{23}^2 c_{12} s_{13} \\
& - c_{12} s_{23}^2 s_{13} s_{12} + c_{12}^2 s_{23} s_{13}^2 c_{23})(-c_{12}^2 c_{23} s_{23} + c_{12} c_{23}^2 s_{12} s_{13} + s_{12} s_{23}^2 s_{13} c_{12} \\
& + s_{12}^2 c_{23} s_{13}^2 s_{23}) \cos \frac{\Delta m_{21}^2}{2E} L + (-s_{12}^2 c_{23}^2 s_{23}^2 c_{13}^2 + s_{12} c_{23}^3 c_{12} s_{13} s_{23} c_{13}^2 \\
& - c_{12} s_{23}^3 s_{13} s_{12} c_{23} c_{13}^2 + c_{12}^2 s_{23}^2 s_{13}^2 c_{23}^2 c_{13}^2) \cos \frac{\Delta m_{31}^2}{2E} L + (-c_{12}^2 c_{23}^2 s_{23}^2 c_{13}^2 \\
& - c_{12} c_{23}^3 s_{12} s_{13} s_{23} c_{13}^2 + s_{12} s_{23}^3 s_{13} c_{12} c_{23} c_{13}^2 + s_{12}^2 c_{23}^2 s_{13}^2 s_{23}^2 c_{13}^2) \cos \frac{\Delta m_{32}^2}{2E} L.
\end{aligned} \tag{A.3}$$

## References

- [1] M. Blasone, F. Dell’Anno, S. De Siena and F. Illuminati, Entanglement in neutrino oscillations, *EPL* **85**, 50002 (2009)
- [2] M. Blasone, F. Dell’Anno, S. De Siena, M. Di Mauro and F. Illuminati, Multipartite entangled states in particle mixing, *Phys. Rev. D* **77**, 096002 (2008)
- [3] M. Blasone, F. Dell’Anno, S. De Siena and F. Illuminati, Hierarchies of Geometric Entanglement, *Phys. Rev. A* **77**, 062304 (2008)
- [4] A. K. Alok, S. Banerjee and S. U. Sankar, Quantum correlations in terms of neutrino oscillation probabilities, *Nucl. Phys. B* **909**, 65-72 (2016)
- [5] S. Banerjee, A. K. Alok, R. Srikanth and B. C. Hiesmayr, A quantum information theoretic analysis of three flavor neutrino oscillations, *Eur. Phys. J. C* **75**, no.10, 487 (2015)
- [6] K. Dixit, J. Naikoo, S. Banerjee and A. K. Alok, Quantum correlations and the neutrino mass degeneracy problem, *Eur. Phys. J. C* **78**, no.11, 914 (2018)
- [7] B. Yadav, T. Sarkar, K. Dixit and A. K. Alok, Can NSI affect non-local correlations in neutrino oscillations?, *Eur. Phys. J. C* **82**, 446 (2022)
- [8] M. J. Molewski and B. J. P. Jones, Scalable qubit representations of neutrino mixing matrices, *Phys. Rev. D* **105**, no.5, 056024 (2022)
- [9] A. B. Balantekin and A. M. Suliga, On the properties of qudits, *Eur. Phys. J. A* **60**, no.6, 124 (2024)
- [10] A. K. Jha, A. Chatla and B. A. Bambah, Neutrinos as qubits and qutrits, *Eur. Phys. J. Plus* **139**, no.1, 68 (2024)
- [11] C.C. Gerry, Nonlocality of a single photon in cavity QED, *Phys. Rev. A* **53**, 4583 (1996).
- [12] S.J. van Enk, Single-particle entanglement, *Phys. Rev. A* **72**, 064306 (2005).
- [13] K. Banaszek, K. Wódkiewicz, Testing Quantum Nonlocality in Phase Space, *Phys. Rev. Lett.* **82**, 2009 (1999).
- [14] H.-W. Lee, J. Kim, Quantum teleportation and Bell’s inequality using single-particle entanglement, *Phys. Rev. A* **63**, 012305 (2000).
- [15] G. Björk, P. Jonsson, L. L. Sanchez Soto, Single-particle nonlocality and entanglement with the vacuum, *Phys. Rev. A* **64**, 042106 (2001).

- [16] A.I. Lvovsky, H. Hansen, T. Aichele, O. Benson, J. Mlynek et al., *Phys. Rev. Lett.* **87**, 050402 (2001).
- [17] T. C. Ralph, A. Gilchrist, G. J. Milburn, W. J. Munro, S. Glancy, Quantum computation with optical coherent states, *Phys. Rev. A* **68**, 042319 (2003).
- [18] M. Pawłowski, M. Czachor, On Entanglement with Vacuum, [quant-ph/0507151](https://arxiv.org/abs/quant-ph/0507151).
- [19] J. Dunningham and V. Vedral, Nonlocality of a Single Particle, *Phys. Rev. Lett.* **99**, 180404 (2007).
- [20] G. Björk, A. Laghaout, and U. L. Andersen, Deterministic teleportation using single-photon entanglement as a resource, *Phys. Rev. A* **85**, 022316 (2012).
- [21] E. Lombardi, F. Sciarrino, S. Popescu, F. De Martini, Teleportation of a Vacuum–One-Photon Qubit, *Phys. Rev. Lett.* **88**, 070402 (2002).
- [22] F. Sciarrino, E. Lombardi, G. Milani, F. De Martini, Delayed-choice entanglement swapping with vacuum–one-photon quantum states, *Phys. Rev. A* **66**, 024309 (2002).
- [23] S. A. Babichev, J. Ries, and A. I. Lvovsky, Quantum scissors: teleportation of single-mode optical states by means of a nonlocal single photon, *Europhys. Lett.* **64**, 1 (2003).
- [24] S. A. Babichev, B. Brezger, A. I. Lvovsky, Remote Preparation of a Single-Mode Photonic Qubit by Measuring Field Quadrature Noise, *Phys. Rev. Lett.* **92**, 047903 (2004).
- [25] S. A. Babichev, J. Appel, A. I. Lvovsky, Homodyne Tomography Characterization and Nonlocality of a Dual-Mode Optical Qubit, *Phys. Rev. Lett.* **92**, 193601 (2004).
- [26] B. Hessmo, P. Usachev, H. Heydari, G. Björk, Experimental Demonstration of Single Photon Nonlocality *Phys. Rev. Lett.* **92**, 180401 (2004).
- [27] K. S. Choi, H. Deng, J. Laurat, H. J. Kimble, Mapping photonic entanglement into and out of a quantum memory, *Nature (London)* **452**, 67 (2008).
- [28] A. Pálffy, C. H. Keitel, J. Evers, Single-Photon Entanglement in the keV Regime via Coherent Control of Nuclear Forward Scattering, *Phys. Rev. Lett.* **103**, 017401 (2009).
- [29] S.-Y. Lee, J. Park, J. Kim, C. Noh, Single-photon quantum nonlocality: Violation of the Clauser-Horne-Shimony-Holt inequality using feasible measurement setups, *Phys. Rev. A* **95**, 012134 (2017).
- [30] D. T. Pegg, L. S. Phillips, S. M. Barnett, Optical State Truncation by Projection Synthesis, *Phys. Rev. Lett.* **81**, 1604 (1998).
- [31] M. Blasone, F. Dell’Anno, S. De Siena and F. Illuminati, Entanglement in a QFT Model of Neutrino Oscillations, *Adv. High Energy Phys.* **2014**, 359168 (2014)
- [32] M. Blasone, F. Dell’Anno, S. De Siena and F. Illuminati, A field-theoretical approach to entanglement in neutrino mixing and oscillations, *EPL* **106**, no.3, 30002 (2014)
- [33] F. Ming, X. K. Song, J. Ling, L. Ye and D. Wang, Quantification of quantumness in neutrino oscillations, *Eur. Phys. J. C* **80**, no.3, 275 (2020).
- [34] A. K. Alok, T. J. Chall, N. R. S. Chundawat and Y. F. Li, Quantifying Imaginarity in Neutrino Systems, [[arXiv:2412.01871](https://arxiv.org/abs/2412.01871)] [[hep-ph](https://arxiv.org/abs/hep-ph)].
- [35] A. Kumar Jha, S. Mukherjee and B. A. Bambah, Tri-Partite entanglement in Neutrino Oscillations, *Mod. Phys. Lett. A* **36**, no.09, 2150056 (2021)

- [36] M. Blasone, S. De Siena and C. Matrella, Wave packet approach to quantum correlations in neutrino oscillations, *Eur. Phys. J. C* **81**, 660 (2021).
- [37] L. J. Li, F. Ming, X. K. Song, L. Ye and D. Wang, Characterizing entanglement and measurement's uncertainty in neutrino oscillations, *Eur. Phys. J. C* **81**, no.8, 728 (2021).
- [38] Y. W. Li, L. J. Li, X. K. Song, D. Wang and L. Ye, Geuine tripartite entanglement in three-flavor neutrino oscillations, *Eur. Phys. J. C* **82**, no.9, 799 (2022)
- [39] Y. W. Li, L. J. Li, X. K. Song and D. Wang, Trade-off relations of quantum resource theory in neutrino oscillations, *Eur. Phys. J. Plus* **137**, no.11, 1267 (2022)
- [40] V. A. S. V. Bittencourt, M. Blasone, S. De Siena and C. Matrella, Quantifying quantumness in three-flavor neutrino oscillations, *Eur. Phys. J. C* **84**, no.3, 301 (2024)
- [41] A. B. Balantekin, M. J. Cervia, A. V. Patwardhan, E. Rrapaj and P. Siwach, Quantum information and quantum simulation of neutrino physics, *Eur. Phys. J. A* **59**, no.8, 186 (2023)
- [42] L. Konwar and B. Yadav, NSI effects on tripartite entanglement in neutrino oscillations, *Nucl. Phys. B* **1002**, 116544 (2024)
- [43] H. Abdolalizadeh and E. Aydiner, Quantum entanglement between neutrino eigenstates in the presence of the subsequent phase shift of the neutrino oscillations, *EPL* **146**, no.5, 54002 (2024)
- [44] V. Giovannetti, S. Lloyd and L. Maccone, Quantum-Enhanced Measurements: Beating the Standard Quantum Limit, *Science* **306**, no.5700, 1330-1336 (2004).
- [45] M. Lostaglio, D. Jennings and T. Rudolph, Description of quantum coherence in thermodynamic processes requires constraints beyond free energy, *Nature Commun.* **6**, no.1, 6383 (2015).
- [46] V. Narasimhachar and G. Gour, Low-temperature thermodynamics with quantum coherence, *Nature Commun.* **6**, no.1, 7689 (2015).
- [47] N. Lambert, Y. N. Chen, Y. C. Cheng, C. M. Li, G. Y. Chen and F. Nori, Quantum biology, *Nature Phys.* **9**, no.1, 10-18 (2012).
- [48] T. Baumgratz, M. Cramer and M. B. Plenio, Quantifying Coherence, *Phys. Rev. Lett.* **113**, no.14, 140401 (2014).
- [49] X. Yuan, H. Zhou, Z. Cao and X. Ma, Intrinsic randomness as a measure of quantum coherence, *Phys. Rev. A* **92**, no.2, 022124 (2015).
- [50] A. Winter and D. Yang, Operational Resource Theory of Coherence, *Phys. Rev. Lett.* **116**,no.12, 120404 (2016).
- [51] L.H. Shao, Z. Xi, H. Fan, Y. Li, Fidelity and trace-norm distances for quantifying coherence, *Phys. Rev. A* **91**, no.4, 042120 (2014).
- [52] T. R. Bromley, M. Cianciaruso and G. Adesso, Frozen Quantum Coherence, *Phys. Rev. Lett.* **114**, no.21, 210401 (2015).
- [53] S. Rana, P. Parashar and M. Lewenstein, Trace-distance measure of coherence, *Phys. Rev. A* **93**, no.1, 012110 (2016).
- [54] X.D. Cui, C.L. Liu, D.M. Tong, Examining the validity of Schatten-p-norm-based functionals as coherence measures, *Phys. Rev. A* **102**, no.2, 022420 (2020).

- [55] F. Yan, T. Gao, X. Qi, Measuring coherence with entanglement concurrence, *J. Phys. A* **50**, no.28, 285301 (2017).
- [56] Z. Xi, S. Yuwen, Coherence measure: Logarithmic coherence number, *Phys. Rev. A* **99**, no.2, 022340 (2019).
- [57] R. Muthuganesan, V. K. Chandrasekar and R. Sankaranarayanan, Quantum coherence measure based on affinity, *Phys. Lett. A* **394**, 127205 (2021).
- [58] Z. Xi and S. Yuwen, Epsilon-smooth measure of coherence, *Phys. Rev. A* **99**, 012308 (2019).
- [59] J. Ma, B. Yadin, D. Girolami, V. Vedral and M. Gu, Converting Coherence to Quantum Correlations, *Phys. Rev. Lett.* **116**, no.16, 160407 (2016).
- [60] Z. Xi, Y. Li and H. Fan, Quantum coherence and correlations in quantum system, *Sci. Rep.* **5**, no.1, 10922 (2015).
- [61] J. K. Asbóth, J. Calsamiglia, and H. Ritsch, Computable Measure of Nonclassicality for Light, *Phys. Rev. Lett.* **94**, 173602 (2005).
- [62] A. Streltsov, U. Singh, H. S. Dhar, M. N. Bera, and G. Adesso, Measuring Quantum Coherence with Entanglement, *Phys. Rev. Lett.* **115**, 020403 (2015).
- [63] W. Vogel and J. Sperling, Unified quantification of nonclassicality and entanglement, *Phys. Rev. A* **89**, 052302 (2014).
- [64] N. Killoran, F. E. S. Steinhoff, and M. B. Plenio, Converting Nonclassicality into Entanglement, *Phys. Rev. Lett.* **116**, 080402 (2016).
- [65] X. K. Song, Y. Huang, J. Ling and M. H. Yung, Quantifying Quantum Coherence in Experimentally-Observed Neutrino Oscillations, *Phys. Rev. A* **98**, no.5, 050302 (2018).
- [66] A. K. Alok, T. J. Chall, N. R. S. Chundawat, S. Gangal and G. Lambiase, Quantum coherence in neutrino spin-flavor oscillations, [arXiv:2407.16742 [hep-ph]].
- [67] I. Esteban, M. C. Gonzalez-Garcia, M. Maltoni, T. Schwetz and A. Zhou, The fate of hints: updated global analysis of three-flavor neutrino oscillations, *JHEP* **09**, 178 (2020).
- [68] D. Collins, N. Gisin, N. Linden, S. Massar and S. Popescu, Bell Inequalities for Arbitrarily High-Dimensional Systems, *Phys. Rev. Lett.* **88**, no.4, 040404 (2002).
- [69] C. Napoli, T. R. Bromley, M. Cianciaruso, M. Piani, N. Johnston and G. Adesso, Robustness of Coherence: An Operational and Observable Measure of Quantum Coherence, *Phys. Rev. Lett.* **116**, no.15, 150502 (2016).
- [70] M. Piani, M. Cianciaruso, T. R. Bromley, C. Napoli, N. Johnston and G. Adesso, Robustness of asymmetry and coherence of quantum states, *Phys. Rev. A* **93**, no.4, 042107 (2016).
- [71] A. C. Doherty, P. A. Parrilo and F. M. Spedalieri, Complete family of separability criteria, *Phys. Rev. A* **69**, no.2, 022308 (2004).
- [72] Q. M. Ding, X. X. Fang and H. Lu, The tightness of multipartite coherence from spectrum estimation, *Entropy* **23**, no.11, 1519 (2021),